Chemical composition of comet C/2007 N3 (Lulin): another "atypical" comet

Proposed running head: Lulin: another "atypical" comet

Erika L. Gibb[1], Boncho P. Bonev[2,3], Geronimo Villanueva[2,3], Michael A. DiSanti[3], Michael, J. Mumma[3], Emily Sudholt[1], Yana Radeva[2,3]

[1] Department of Physics & Astronomy, University of Missouri - St Louis, St Louis, MO, 63121, USA

[2] Department of Physics, The Catholic University of America, Washington, DC 20064, USA

[3] Goddard Center for Astrobiology, Solar System Exploration Division, NASA Goddard Space Flight Center, code 690, Greenbelt, MD 20771, USA

Submitted to Astrophysical Journal December 29, 2011

Editorial correspondence and proofs should be directed to ELG

Erika Gibb

503 Benton Hall

One University Blvd

University of Missouri – St. Louis

St. Louis, MO 63121

Phone: (314) 516-4145

Fax: (314) 516-6152

E-mail: gibbe@umsl.edu

Abstract

We measured the volatile chemical composition of comet C/2007 N3 (Lulin) on three dates from 30 January to 1 February, 2009 using NIRSPEC, the high-resolution ($\lambda/\Delta\lambda \approx 25{,}000$), long-slit echelle spectrograph at Keck 2. We sampled nine primary (parent) volatile species (H_2O, C_2H_6, CH_3OH, H_2CO, CH_4, HCN, C_2H_2, NH_3, CO) and two product species (OH* and NH_2). We also report upper limits for HDO and CH_3D. C/2007 N3 (Lulin) displayed an unusual composition when compared to other comets. Based on comets measured to date, CH_4 and C_2H_6 exhibited "normal" abundances relative to water, CO and HCN were only moderately depleted, C_2H_2 and H_2CO were more severely depleted, and CH_3OH was significantly enriched. Comet C/2007 N3 (Lulin) is another important and unusual addition to the growing population of comets with measured parent volatile compositions, illustrating that these studies have not yet reached the level where new observations simply add another sample to a population with well-established statistics.

Keywords: Astrobiology; Comets: individual: C/2007 N3 (Lulin); Methods: observational Techniques: spectroscopic; solar system – ISM: molecules – solar system: formation

1. Introduction

Cometary nuclei are arguably the most primitive bodies formed in the outer solar system (beyond ~5 AU), and therefore studies of their chemical composition have cosmogonic implications. The standard model of cometary origins suggests that most cometary nuclei now residing in the Kuiper Disk formed in our planetary system at distances beyond ~ 5 AU, though the "Grand Tack" model (Walsh et al. 2011) suggests that many might have originated in the terrestrial planets region. Whether Oort Cloud comets formed solely in our planetary system or were also captured from neighboring stars in the Sun's birth cluster (Levison et al. 2010) is also in play. Resolving these key questions promises insights into processes that actually happened, but will require the combined insights provided by dynamical models for realistic solar system analogues, and by measurements of composition and related cosmogonic parameters. Here, we advance that goal by measuring primary (parent) volatiles in comet C/2007 N3 (Lulin).

There is increasing evidence of various processes that may have altered the primordial composition of comets since emplacement in their current reservoirs (cf. Stern, 2003; Weissman et al., 2004). The majority of these processes are believed to affect a (primarily) thin layer at the surface of the nucleus. For example, cosmic rays may have modified the chemistry of the outer surface (to a depth of perhaps a few meters) during a comet's long storage in the Oort Cloud, the passing of nearby hot (O or B) stars or supernovae could have thermally modified the top few meters of material, and interstellar grain collisions may have mechanically sputtered the surface layer (see Stern, 2003 for a more detailed discussion of evolution mechanisms in the Oort Cloud). After ejection from the Oort Cloud, warming on repeated passes through the inner solar system could induce surface changes. However, it is generally believed that comets lose several meters of material during each apparition, so that any chemically altered layers are likely lost.

Even in the case of a dynamically new comet from the Oort Cloud, post-perihelion measurements of gas production (such as those reported here) should be representative of the more primitive nuclear composition.

When interpreted in the context of chemical disk models and current observations of proto-planetary disks, we begin to unravel the processes that influenced the formation and history of cometary volatiles. If we are measuring the original composition of cometary material, then it follows that information about the formation environment of a comet could be deduced from the overall volatile composition, including relative abundances of organic volatiles (e.g., CH_4/H_2O, HCN/H_2O, etc.), D/H ratio in water and methane, and possibly nuclear spin temperatures. New models suggest that dynamical mixing in the early solar system placed comets of differing origins into the Oort Cloud, possibly even icy bodies from other stars in the natal cloud from which the solar system formed (Levison et al. 2010). Hence, by studying a large number of comets, we should sample a variety of formation environments.

Studies on species produced in the coma have suggested that comets from the Oort Cloud and Kuiper Belt exhibit a rich compositional diversity that seems to correlate somewhat with the reservoir from which the comet originated, at least for some molecules (A'Hearn et al. 1995; see Schleicher 2008; Fink 2009 for recent developments). However, the fragment species in those studies have uncertain precursors, clouding the possible interpretations in terms of volatiles in cometary nuclei. In the infrared, observations of primary volatiles in a small number of objects (less than two dozen) have suggested (as a working hypothesis) compositional classes of "normal", "organics-rich", and "organics-poor". However, some recently observed comets have been found to differ uniquely in composition and don't appear to fit neatly into a simple classification scheme (e.g., 8P/Tuttle: Bonev et al. 2008, Boehnhardt et al. 2008, Kobayashi et al.

2010; and C/2000 WM_1: Radeva et al. 2010). For a recent review of compositional taxonomies and possible natal heritage, see Mumma and Charnley (2011).

Here, we report the volatile composition of Oort Cloud comet C/2007 N3 (Lulin). We measured the comet soon after its perihelion passage, by which time any chemically altered surface layer was likely lost. Section 2 discusses our observations and data analysis. Our results are given in section 3 and discussed in detail in context of the comet population in section 4. Our overall conclusions are discussed in section 5. Like 8P/Tuttle, C/2007 N3 (Lulin) appears to be an Oort Cloud comet of distinct composition.

2. Observations and Data Analysis

Comet C/2007 N3 (Lulin) was discovered on 11 July 2007 by Ye Quanah and Lin Chi-Shang at the Lulin Observatory (Young 2007). C/2007 N3 (Lulin) had an original 1/a of 0.000021, corresponding to an aphelion distance of approximately 95,000 AU (Nakano 2011; Nakano's current orbital solution is based on observations from 11 July 2007 to 2 October 2010). The original (Jupiter) Tisserand parameter of -1.24 (now -1.365) indicates that C/2007 N3 (Lulin) is from the Oort Cloud, and its large aphelion distance suggests that the recent apparition was its first journey to the inner solar system since its emplacement in the Oort cloud (i.e., it might have been dynamically new). In 2009, it reached perihelion (1.22 AU) on January 10.6 and its closest approach to Earth (0.41 AU) on 24.3 February. We observed the comet shortly after perihelion and shortly before closest approach.

We quantified the overall volatile composition of comet C/2007 N3 (hereafter Lulin) on January 30-February 1, 2009, via spectra acquired with NIRSPEC at the 10-meter W. M. Keck Observatory (McLean et al. 1998). Our observing log is shown in Table 1. On these dates, Lulin had an unusually large geocentric Doppler shift (exceeding 50 km s^{-1}), placing lines of molecules

having opaque telluric counterparts (in particular CO and (especially) CH_4) in regions of high transmittance. Observations were performed with a 3-pixel (0.43″) wide slit, permitting acquisition of high spectral resolution data ($\lambda/\Delta\lambda \sim 25{,}000$). We used our standard ABBA nod pattern, with a 12″ beam separation along the 24″ long slit. Combining the spectra of the two beams as A-B-B+A cancels instrumental biases and also emissions from "sky" lines and thermal background to second order, in a Taylor Series expansion about the mean air mass.

[Table 1]

Data were processed using custom algorithms to achieve dark subtraction, flat fielding, and removal of high dark current pixels and cosmic ray hits. Detailed descriptions of the reduction procedures and flux calibration (achieved through observations of infrared standard star BS 4689) can be found in Villanueva et al. (2011b), Radeva et al. (2010), Bonev (2005 – Appendix 2) and references therein. Atmospheric spectra were synthesized using the LBLRTM (Line-By-Line Radiative Transfer Model, Clough et al. 2005), which was optimized for Mauna Kea's atmospheric conditions (see Villanueva et al. 2011a). We used these models to assign wavelength scales to the extracted spectra and to determine column burdens for the absorbing species in the Earth's atmosphere. The atmospheric model was binned to the resolution of the comet spectrum, normalized, and scaled to the comet's continuum level. The residual cometary line fluxes were obtained by subtracting the atmospheric model from the processed cometary spectra (row-by-row), and the measured residual fluxes for cometary emission lines were then corrected for the monochromatic transmittance at the Doppler-shifted position of each line. Line-by-line spectral identifications, rest frequencies, and transmittance-corrected fluxes are provided in Table 4.

Symmetric production rates (in molecules s^{-1}) were calculated at regular intervals along the slit by assuming the idealized case of spherically symmetric outflow at uniform velocity, $v_{gas} = 0.8R_h^{-0.5}$ km s^{-1}. A symmetric Q-curve was constructed from the mean emission intensity (averaged to either side of the nucleus) measured in 0.6-arcsec intervals along the spatial direction of the slit according to:

$$Q = \frac{4\pi\Delta^2 F_i}{g_i \tau (hc\nu) f(x)}, \quad (1)$$

(see Bonev 2005, pp. 74-83; Dello Russo et al. 1998, 2000; Magee-Sauer et al. 1999; and DiSanti et al. 2001 for more details). Here Δ is the geocentric distance in meters, $hc\nu$ is the energy (J) of a photon with wavenumber ν (cm^{-1}), f(x) is the fraction of molecules expected in the sampled region (see appendix of Hoban et al. 1991), and F_i is the flux (W m^{-2}) from line *i* incident on the terrestrial atmosphere. The photo-dissociation lifetime (τ) is taken from the quiet Sun values in Huebner et al. (1992) for each molecule, and g_i is the line fluorescence efficiency (photons s^{-1} $molecule^{-1}$), both of which were calculated for the comet's heliocentric distance at the time of our observations.

The symmetric Q increases with distance from the nucleus owing to atmospheric seeing, comet drift, and other observing factors, until reaching a terminal value that we take to be the "global" production rate. An example Q-curve is shown in Figure 1. When using this method, the derived production rates are less sensitive to seeing, drift of the comet perpendicular to the slit, and potential optical depth effects in the coma.

[Figure 1]

Our fluorescence efficiencies (g-factors) are based on individual quantum mechanical models for each molecule: CH_4 (Gibb et al. 2003), C_2H_6 ν_7 (Villanueva et al. 2011a), C_2H_6 ν_5 (Radeva et al. 2011), H_2O and HDO (Villanueva et al. 2012), OH* (Bonev et al. 2006), CH_3OH (Villanueva et al. 2011c), H_2CO (DiSanti et al. 2006), NH_2 (Kawakita & Mumma 2011), C_2H_2 and CO (Villanueva et al. 2011b), NH_3 (Kawakita & Mumma 2011; Villanueva et al. 2011d) and

HCN (Lippi et al. in prep; Villanueva et al. 2011d). We have also incorporated a more realistic solar pumping flux (Villanueva et al. 2011a) rather than the blackbody assumed in previous modeling efforts.

3. Results

We detected 9 primary volatiles (often referred to as parent volatiles in earlier literature) in comet Lulin: H_2O, CO, CH_4, C_2H_6, CH_3OH, H_2CO, HCN, C_2H_2, and NH_3. We also sampled two deuterated primary species (HDO and CH_3D) and two product species (NH_2 and OH* -the "*" denotes dissociatively-excited hydroxyl) and NH_2. Spectra and best-fit fluorescent emission models for the rotational temperatures (see section 3.1) and production rates of Table 2a are shown in Figures 2-7. We used a Levenberg-Marquardt non-linear minimization technique to simultaneously fit fluorescent emission models of all species (see Villanueva et al. 2011b for details). In all cases, we found consistent results and excellent fits to the comet spectra (see Table 2a and Figures 2-7) and are confident that our retrievals of production rates and rotational temperatures are robust.

[Figures 2-7]

3.1 Rotational Temperatures

We retrieved rotational temperatures using correlation and excitation analyses explained in detail in Bonev (2005, pp. 53-65), Bonev et al. (2008b), DiSanti et al. (2006), and Villanueva et al. (2008). Rotational temperatures can be accurately determined for molecules that sample a broad range of excitation energies, a condition that was satisfied for H_2O, CH_4, HCN, and CO. For these molecules, the rotational temperatures were generally found to have uncertainties of 1-5 K and were usually in agreement with each other (see Table 2a). C_2H_6 and CH_3OH generally have higher uncertainties in the retrieved rotational temperatures (on the order of 10 K) due

primarily to spectral confusion. For the remaining molecules, we assumed a rotational temperature consistent with that found for the well-sampled molecules. This approach is valid, considering that in most cases rotational temperatures derived from IR observations are in reasonably good agreement among various species. However, for some molecules/dates we report results for both the best fit to the measured spectrum of the molecule and for the assumed T_{rot} (denoted in parenthesis). Note that when we sample a broad range of excitation energies, slight changes in T_{rot} result only in very small differences in production rates and mixing ratios (Table 2a), adding confidence to our results.

3.2 Volatile Abundances – Comparison to Current Composition End Members

Relative abundances (mixing ratios) were determined by comparing the production rate of each molecule to that found for H_2O on the same date and within the same NIRSPEC setting. Since NIRSPEC has very large spectral coverage for each instrument setting, trace molecules were observed simultaneously with H_2O, resulting in very well constrained mixing ratios. A comparison with current median values of abundances (relative to H_2O) measured in other comets in the infrared provides three principal results:

1. C_2H_2 and H_2CO have very low abundances, while CO and HCN are moderately depleted,
2. CH_4 and C_2H_6 have abundances close to the current median values,
3. CH_3OH has one of the highest abundances observed to date.

Acetylene, which is often comparably abundant to HCN, was especially depleted in Lulin (0.05-0.08%). This was so even on 1 Feb when the overall production rates were significantly higher than on the previous two nights. This is illustrated in Figure 8, which shows abundance ratios relative to a reference value. Since we have not fully sampled the comet population, the median abundances often change with new observations. Hence, we define the reference as in Villanueva

et al. (2011b). It is heavily weighted to C/1996 B2 (Hyakutake), C/1995 O1 (Hale-Bopp), and C/1999 H1 (Lee) for which we have the most precise measurements to date at IR wavelengths. Comet Lulin is compared to the current compositional end members C/2001 A2 (LINEAR), C/2001 W1 (Boattini), and C/1999 S4 (LINEAR). Importantly, in these three comets, the degree of "enrichment" or "depletion" is correlated among all measured volatiles. Among comets measured to date, Comet C/1999 S4 (Mumma et al. 2001) is a compositional end member because its abundances are systematically much lower than the median for each species, while C/2001 A2 (Magee-Sauer et al. 2009) and Boattini (Villanueva et al. 2011b) show mixing ratios that are systematically on the high end. We do note that Boattini exhibited an unusual outflow pattern suggesting a component of nearly pure polar (water + methanol) ice grains emitting primarily in the anti-sunward direction (see Figure 5 in Villanueva et al. 2011b). If abundances are determined from the mixed-ice moiety component, only CH_3OH and, to a lesser extent C_2H_6, are enriched in Boattini. In general, we can thus classify C/1999 S4 as "organics-depleted", while A2 and Boattini are examples of "organics-enriched" comets. The composition of comet Lulin cannot be described through simply an overall enrichment or depletion of trace species relative to H_2O. In particular, compare the large differences among CH_3OH, CH_4, C_2H_2, and HCN in Lulin, from more abundant to much less than the median in Figure 8.

[Figure 8]

The oxygen bearing species show particularly unusual abundance ratios. For H_2CO, we found an abundance of ~0.1% over the three nights (Table 2a). We note that the ν_1 Q-branch near 2781 cm^{-1} seems underestimated in the model and when analyzed alone, results in a slightly higher abundance of ~0.2% (see Figure 5; Table 2a, footnote 'd'). The reason for this is unknown. However we note that nearby spectral regions (in KL2 order 21) contain emissions in

Lulin not predicted by the model (e.g., near 2801 cm^{-1}), and similarly excess (i.e., unaccounted for) emission may also be blended with the Q-branch. We take the lower value (0.1%) to be our most probable abundance, since it is based on multiple H_2CO features in order 21. DiSanti et al. (2006) found good agreement among the Q branch and other lines in comet C/2002 T7, for which the abundance ratio H_2CO/H_2O (~ 0.75-0.94%) was much higher than we observed in Lulin. Regardless of model uncertainties, we can conclude that H_2CO is relatively depleted in Lulin.

In Lulin, the CO abundance ratio (2.2%) is slightly below the median value (~4%) among Oort Cloud comets, though it is well within the wide range of values observed to date. CH_3OH, by contrast, is unusually abundant in Lulin (~3.6%), nearly double the median value of ~2%. Lulin's oxygen chemistry is similar to that of comet C/2007 W1 (Boattini), which also displayed low H_2CO (<0.12%), close to median CO (4.3%) and high CH_3OH (~3.9%), although Lulin does not display the enhanced abundances in nitrogen-bearing species (HCN, NH_3) and C_2H_6 that were seen in Boattini (Villanueva et al. 2011b).

We also detected NH_3 in Lulin, but only on 1 Feb - there is no evidence of NH_3 emission in our spectra taken on 30 Jan and 31 Jan. The teal tick marks above the top spectrum in Figure 2 indicate the expected positions of the two strongest NH_3 lines. In particular, note the expected position (and non-detection) of the blended sqP(3,0) and sqP(3,1) lines near 3278 cm^{-1}. We detected this blend on 1 Feb, along with the aP(2,0) and aP(2,1) blend near 3296 cm^{-1} (Figure 3). We determined 3-sigma upper limits of 0.19% and 0.22% on 30 and 31 Jan, respectively, and an abundance of 0.25 ± 0.05% on 1 Feb, within 1-sigma of our upper limits on the previous two nights (Table 2a). This difference is consistent with the overall higher gas production of Lulin

on 1 Feb (by a factor of about two), which improved the signal-to-noise by enough to detect emissions from NH_3.

3.3 Compositional Variability in Comet Lulin

Another interesting aspect of our data is the evidence of variability of certain molecules. The overall water production rate varied over the nights of our NIRSPEC observations, which for some comets can be explained as jets rotating into or out of the line of sight. Lulin was found to vary with a period of 42.0 hours with two side-on gas jets rotating in a corkscrew morphology (Knight & Schleicher 2009), making a jet explanation for night-to-night variability a plausible explanation. If the nuclear ice composition were homogeneous and well represented by the material released from jets, we would expect the production rates of trace molecules to follow that of water. In some cases, this holds. For example, H_2CO abundances agree to within uncertainty on all three nights, while there seems to be a slight progressive decrease in the abundances of HCN, C_2H_2, and CH_4 from 30 Jan to 1 Feb (see Figure 9). We note that changes in T_{rot} are not responsible, since such changes have a small effect on the overall production rate (see section 3.1 and Table 2a). Changes in the water production rates are also not solely responsible, since they were lower (higher) than the 30 Jan value on 31 Jan (1 Feb), respectively. Also, as noted above, H_2CO (observed on all three nights) did not exhibit abundance variations even though the overall gas production rate varied by more than a factor of two (Table 2a).

[Figure 9]

3.4 Production Rate Variability in Comet Lulin

The overall productivity of Lulin varied significantly over the time encompassed by our observations (Table 2a, Figure 9), with overall water production rates of 1.35×10^{29} (1.13×10^{29}) molecules s^{-1} on 30 Jan (31 Jan) respectively. Such variations are expected in comets that show

active jets, like Lulin, since nucleus rotation can change the production rate. Of particular interest is the production rate of water on 1 Feb. Tables 1 and 2a show the settings in the order in which they were observed (KL1, MW-A, MW-C, KL2). There was a steady increase in production rate over the course of the night (from 1.6-2.5x10^{29} molecules s^{-1}). The production rates of all molecules increased. For example, we sampled both H_2O and CO in MW-A and MW-C. While the total production rates increased, the abundance ratios remained the same within the uncertainty. Similar behavior was observed in 103P/Hartley 2, the first comet for which the interpretation of such rotation-modulated production rates was supported by direct imaging of release from the nucleus (A'Hearn et al. 2011; Mumma et al. 2011). For this reason, we determined abundances strictly by comparing production rates for traced molecules and water observed simultaneously in each setting. These are the values reported in Table 2a.

3.5 Cosmogonic Indicators of Comet Lulin

3.5.1 Spin Temperature

In addition to relative volatile abundances, there are two parameters that are thought to possibly represent cosmogonic cometary quantities that have remained unchanged since the formation of the comet and, if so, could provide information about, for example, formation temperature of the volatile component. These two parameters are the spin temperature and the D/H ratio. In molecules containing identical nuclei (such as H_2O) the nuclear spins can be oriented in parallel (ortho-H_2O) or anti-parallel (para-H_2O) configurations. Conversion between spin species is strictly forbidden for radiative or neutral-neutral collisions (Hougen & Oka 2005; Mumma et al. 1987) and hence gas phase collisions in the coma should not change the ortho-to-para ratio of cometary volatiles (supported by Bonev et al. 2007, see their Figure 2). The nuclear spin temperature is therefore considered a key measurement for determining the formation

temperature of cometary water. (Nuclear spin temperatures for H_2O and NH_3 are similar in comets for which both primary volatiles have been measured, even though their OPR ratios are quite different. See the review by Mumma & Charnley 2011.)

The lowest energy level of para-H_2O lies 23.8 cm^{-1} (~34 K) below the lowest ortho level. Hence, if cometary water formed at very low temperatures, we should be able to infer this by measuring the ortho and para populations, with the critical assumption that they have remained unchanged in the nucleus since their formation. At higher spin temperatures (above $T_{spin} \approx 45$ K) the ratio approaches the statistical equilibrium value of 3.0. Figure 10 shows a sample water spectrum toward Lulin taken on 31 Jan. 2011. The best-fit model spectra for the ortho (red) and para (purple) lines are shown. Also shown for completeness is OH (blue). For Lulin, we determined an OPR of 3.17±0.12 (1-sigma uncertainty, dominated by the standard error in the line-by-line distribution) on 31 Jan, consistent with statistical equilibrium and corresponding to spin temperatures higher than ~45 K.

Our result differs from the frequently reported T_{spin}~30 K found for many comets (Kawakita et al. 2006; Dello Russo et al. 2005; Crovisier 2000; Mumma et al. 1987) although other comets, such as C/2007 W1 Boattini (Villanueva et al. 2011b), 73P/Schwassmann-Wachmann 3-B (Bonev et al. 2008b; Dello Russo et al. 2007), and C/1999 S4 (Dello Russo et al. 2005) have water ortho-to-para ratios consistent with statistical equilibrium, or at least T_{spin} higher than 30 K (e.g., C/2004 Q2 (Machholz), Bonev et al. 2009). The results suggest, not surprisingly, a variety of formation environments for cometary bodies. We will report spin temperatures for comet Lulin on all three dates in a comprehensive upcoming paper describing in detail the ortho-para ratio analysis in detail.

[Figure 10]

A similar analysis was performed for CH_4, which contains three spin species (denoted A, E, and F with statistical equilibrium abundance ratios of 5:2:9, respectively). Unlike water, for which "pure" ortho and para lines can be measured, the CH_4 analysis is complicated by the fact that spectral lines of the individual spin species are blended at the spectral resolution of NIRSPEC. The exceptionally large geocentric Doppler shift of comet Lulin permitted us to sample nine transitions of CH_4. We used the overall spectrum to determine the rotational temperature of CH_4, which we found to be consistent with that measured for water, and then we used the R0 and R1 lines, which are pure A and F transitions, respectively, to determine the spin temperature, performing an iterative procedure until the best fit synthetic spectrum was reached (similar to the procedure applied to H_2O by Bonev et al. 2008). We confirmed our results by also determining the spin temperature over the entire spectrum (versus the R0 and R1 lines only) and found consistent results. The resulting model spectrum for 30 Jan. (with each spin component modeled separately) and corresponding excitation analysis is shown in Figure 11. We achieved a very good fit for T_{rot} = 65 K and T_{spin} > 60 K (statistical equilibrium).

[Figure 11]

If we assume that spin temperature is indicative of the formation temperature, then the spin temperatures for water and methane imply that the bulk of the volatile material in comet Lulin was formed at temperatures exceeding ~50 K. This would place the volatiles within a region of about 8 AU from the young Sun, according to predicted mid-plane temperatures in the models by Walsh et al. (2010) and Willacy & Woods (2009). We do note that radial and vertical mixing into the mid-plane can inject material that formed at warmer temperatures (in the disk atmosphere) and/or at larger heliocentric distances. The CH_4 and H_2O in Lulin could have formed, for example, in a warm molecular layer above the mid-plane at larger distances and then

have been transported to the mid-plane (through turbulent mixing) prior to freezing onto grains. We discuss such scenarios in more detail in section 4.

3.5.2 Deuterium Abundance

The ratio of D/H in a particular molecule is also temperature dependent at the low temperatures expected in the plausible formation environment of cometary molecules. HDO has been measured in only five comets: Halley, Hyakutake, Hale-Bopp, 8P/Tuttle and 103P/Hartley 2 (Eberhardt et al. 1995; Bockelée-Morvan et al. 1998; Meier et al. 1998; Villanueva et al. 2009; Hartogh et al. 2011) with results indicating a range of D/H values in comets (for a recent review, see Mumma & Charnley 2011).

We searched for HDO and CH_3D in Lulin, but did not detect either species (a detailed discussion of the analytical procedures is in preparation). Here we quote our results and discuss possible implications in order to provide a more comprehensive view on comet Lulin. The D/H ratio in water was found to be $< 5.6 \times 10^{-4}$ (3-sigma), corresponding to an upper limit of 3.6 VSMOW (where VSMOW is the D/H value in Vienna Standard Mean Ocean Water) from only 36 minutes on source integration time. This is a significant upper limit given the moderate brightness of Lulin, and demonstrates that reaching 1.55×10^{-4} (1 VSMOW) sensitivity is viable in moderately active comets with NIRSPEC. A useful empirical scale for the intensity of molecular infrared lines in a comet is the so-called "figure of merit", FoM, commonly used to plan observations (e.g., see Mumma et al. 2003). Comet Lulin had an infrared "figure of merit" of 0.85 (Jan. 31, 2009). For comparison, Hale-Bopp and Hyakutake reached figures of merit ~80 and ~20, respectively.

Our CH_3D/CH_4 3-sigma upper limit (see Figure 12) is 3.0% on 30 Jan and 2.9% on 31 Jan, similar to the upper limits reported for C/2001 Q4 (NEAT) (4%, Kawakita et al. 2005) and

for C/2004 Q2 (Machholz) (2%, Bonev et al. 2009; 2.6%, Kawakita & Kobayashi 2009). So far all these values, like those for HDO, are not consistent with an unmodified cold, dark cloud origin for cometary volatiles (see Discussion).

[Figure 12]

4. Discussion

Cometary abundances are often compared with interstellar medium values, particularly to ice absorption studies toward protostars. In a general sense, the abundances of key ice species in comets, such as CO, CH_4, CH_3OH, and H_2CO are within the range of values observed in YSOs (see Mumma & Charnley 2011 for a review). This may suggest that the overall abundances of volatiles in comets are dominated by grain surface chemical reactions and adsorption prior to disk formation. Such a comparison may be overly simplistic, however. Ice compositions in dark clouds can vary for some species along different lines of sight. For example, CH_3OH varies from <1% to ~15% toward low mass young stars (Pontoppidan et al. 2003; Boogert et al. 2008) and up to 12% through cold dark clouds (Boogert et al. 2011). CO_2 varies from a few to ~35% relative to water ice towards protostars (Gerakines et al. 1999, Nummelin et al. 2001, Pontoppidan et al. 2008, Cook et al. 2011). Absorption features from species like HCN, C_2H_2, and CH_4, are difficult to detect in the ice. CH_4 has only been detected in a few objects to date (Gibb et al. 2004; Öberg et al. 2008) and C_2H_2 and HCN have not been convincingly detected (Boudin et al. 1998).

4.1 Comparison with astrochemical models

In cold, dense interstellar clouds, H atom addition reactions on grain surfaces favor an enrichment in deuterium for both methane and water. Predicted values for D/H in molecules formed in dark clouds at low (~10 K) temperatures are quite high. For example, Willacy and Woods (2009) predict HDO/H_2O ~ 1% and Aikawa and Herbst (1999) predicted CH_3D/CH_4 = 9-

20%. Millar et al. (1989) predicted CH_3D/CH_4 = 2% assuming a dense molecular cloud at 30 K. Our upper limits of D/H in both methane and water are lower than most of these predictions, i.e., our results do not support the hypothesis that material from a 10-20 K dark cloud was incorporated without processing into comet Lulin. However, if comets are comprised at least in part of material that formed (or was processed) in the inner solar nebula and subsequently underwent radial mixing, then the deuterium ratio in molecules might be lowered to values consistent with our results.

Processing of volatiles after incorporation into the proto-planetary disk might also be an important contributor to the observed distinct abundance differences among comets, with some molecules varying, relative to water, by more than an order of magnitude. Many models predict that ice mantles will be evaporated by shock heating upon infall to the disk. It is constructive, therefore, to compare observed organic abundances in comets to recent proto-planetary disk models (e.g., Willacy & Woods 2009; Walsh et al. 2010). These models generally divide the disk into three main regions: **(1)** a *cold mid-plane*, where molecules freeze onto dust grains (modeled abundances for the mid-plane are most suitable for direct comparison with our observations); **(2)** a *warm molecular layer,* where ices sublimate from interstellar grains and are then processed via gas-phase reactions, involving radicals and ions that are produced by the proto-stellar radiation field; these reactions are predicted to synthesize species like HCN, C_2H_2, H_2CO, CH_4, and H_2O and **(3)** *a hot disk atmosphere* (at the nebular surface) containing predominantly atoms and atomic ions rather than radicals. What is important, with regard to interpreting comet volatile abundances, is how these regions interact.

According to Walsh et al. (2010), C_2H_2, HCN, and H_2CO are produced in a thin warm molecular layer. In this model, extreme mid-plane depletion of the gas-phase abundances of

these molecules is predicted owing to vertical mixing to the mid-plane with gas freezing onto the grains. For HCN, this happens beyond about 4.3 AU. Water condenses beyond ~2 AU, and H_2CO beyond 1.5 AU. Interestingly, the relatively warm mid-plane temperatures (in the model) imply that CO should not condense in the mid-plane throughout most of the disk, contrary to the occasionally abundant CO measured in cometary comae.

One thing is clear when analyzing volatiles in comets. The relative abundances do not scale according to binding energy. In Lulin, for example, H_2CO (with a H_2CO-H_2CO binding energy, E_D, of 1760 K, Tielens & Allamandola 1987) is depleted relative to the enriched CH_3OH (E_D (CH_3OH-CH_3OH) = 4240 K, Sandford & Allamandola 1993). However, the hypervolatile CO (E_D (CO-CO)= 855 K, Öberg et al. 2005) is not severely depleted. In interstellar ices, production of H_2CO and CH_3OH in ice mantles follows from hydrogenation reactions of CO with ambient H, likely during the polar mantle formation phase (Whittet et al. 2011). If gas phase reactions in the protoplanetary disk can be ignored, a high abundance of CH_3OH and a low abundance of H_2CO may imply a high efficiency of conversion from $H_2CO + H \rightarrow CH_3OH$ in cometary ices. DiSanti et al. (2009) suggested similar high conversion efficiency for C/2006 M4 (SWAN). However, we may also be sampling the results of chemistry in a warm molecular layer followed by turbulent mixing. Thus far, most chemical models do not incorporate full radial mixing or vertical turbulence, though Heinzeller et al. (2011) have incorporated diffusion and turbulent vertical mixing. To better understand the chemistry leading up to comet formation, much more work is needed, both on modeling as well as measuring cometary abundances.

4.2 Comparison with product species abundances

Optical observations target species such as CN, C_2, and OH, which can be photo-dissociation products of HCN, C_2H_2, and water, respectively. Dust grains and other volatiles

species (such as C_2H_6) have also been suggested as possible contributors to C_2 and CN (e.g., A'Hearn et al. 1995), though their contribution is difficult to assess without knowing the dust composition. A comparison of relative production rates, for example CN/OH and HCN/H_2O, can test the possible chemical pathways in the coma of a comet and indicate whether additional sources for product species are needed to explain their production in the coma (see Table 3).

Production rates for the product species CN, C_2, and OH in Comet Lulin were reported by Bodewits et al. (2011) using data acquired on 28 January 2009 with the Ultraviolet and Optical Telescope on board the Swift gamma-ray burst space observatory. Using their product species and our parent species production rates, we find (assuming no nuclear heterogeneity) that the CN/OH and HCN/H_2O ratios are similar in Lulin, meaning most (if not all) of Lulin's CN may originate from HCN, similar to the findings of Paganini et al. (2010) for 73P/Schwassmann-Wachmann 3. This is not always the case, with some comets exhibiting higher relative production rates for CN than for HCN, and for C_2 than for C_2H_2, as in 8P/Tuttle (Bonev et al. 2008, see also Cottin & Fray 2008; Fray et al. 2003, 2005; Dello Russo et al. 2009). This indicates that an additional primary species (dust or gas) is necessary to explain the production of CN in some comets.

The situation is similar in comet Lulin (Table 3). Much more C_2 is produced in the coma than can be explained by photo-dissociation of C_2H_2, which is depleted in Lulin. The spatial profile of C_2 often suggests that a complex chemistry involving multiple photo-dissociations is needed (see for example Fink et al 1991; Combi et al. 1986). It has been suggested that C_2H_6, which photo-dissociates into C_2H_5 and C_2H_4, may also contribute to C_2 (Helbert et al. 2005; Kobayashi et al. 2010). C_2H_5 and C_2H_4 photo-dissociate to C_2H_2 and then to C_2, with branching ratios that, while uncertain, have been estimated to provide up to a 50% yield of C_2 from C_2H_6

(Kobayashi et al. 2010; Helbert et al. 2005). If we include a possible C_2H_6 contribution, we find that C_2H_2 and C_2H_6 could potentially account for most of the C_2 production for comet Lulin. However, given the unknown branching ratios, the contribution of C_2H_6 to C_2 should be considered highly uncertain.

This consistency between volatile HCN, C_2H_2, and C_2H_6 with product species CN and C_2 is not generally found. For example, Kobayashi et al. (2011) and Bonev et al. (2008) found that HCN, C_2H_2, and C_2H_6 could not account for the abundances of CN and C_2 in the Halley family comet 8P/Tuttle. Dello Russo et al. (2009) also found insufficient HCN, C_2H_2, and C_2H_6 to account for CN and C_2 in the coma for Jupiter family comet 6P/d'Arrest. These results suggest an additional source is needed to produce C_2, and sometimes CN, in cometary comae, possibly CHON grains. While we cannot rule out an additional source such as CHON grains for CN and C_2, our results would seem to suggest that this additional source is less abundant in Lulin than in 8P/Tuttle or 6P/d'Arrest.

4.3 Compositional Variability

Given the suggestion of compositional variability in Lulin, it is worth considering other evidence for or against heterogeneity in the comets observed to date. Heterogeneity can be tested in two primary ways: (1) observing several components of a single comet that fragmented into several pieces, hence directly sampling multiple components of a single comet, or (2) observing a single comet on multiple dates, thereby (potentially) sampling release from different active regions. Such observations have been performed toward several comets, and for the most part, comets have been found to be homogeneous to within the observational uncertainties. For example, Villanueva et al. (2006) and Dello Russo et al. (2007) reported abundances of the same species targeted in two components of the fragmented comet 73P/Schwassmann-Wachmann 3

(components B and C). They found that both components had very similar compositions, which suggests that variations seen among the comet population in, for example, carbon chain molecules are primordial. Comet C/2004 Q2 (Machholz) was observed two months apart, in November 2004 (Bonev et al. 2009) and in January 2005 (Kobayashi et al. (2009); Bonev et al. 2009). The mixing ratios for most molecules (with the possible exceptions of CH_4 and CH_3OH) were found to agree, even though the overall productivity of Comet Machholz was significantly different. Similarly, mixing ratios in 8P/Tuttle agreed well although measured on different dates (Boehnhardt et al. 2008; Bonev et al. 2008; Kobayashi et al. 2010). And, for 103P/Hartley 2, nucleus rotation caused production rates to change by a factor of two in nine hours, but mixing ratios were unchanged then and also over a span of three months (Mumma et al. 2011). These results suggest that most comets have not exhibited evidence of large-scale chemical heterogeneity.

However, there are notable exceptions. Comet C/2001 A2 (LINEAR) was observed in July and August 2001. Gibb et al. (2007) reported a significant change in the abundance of H_2CO from 0.3% on 9.5 July to 0.05% on 10.5 July. CH_4 varied from ~1.5% in July to 2.9% in August. Also, Mumma et al. (2005) and DiSanti et al. (2007) noted a factor of 2-3 increase in the C_2H_6 abundance in 9P/Tempel 1 after the Deep Impact mission ejected material from the subsurface. More recently, Mumma et al. (2011) reported distinctly different outflow properties among volatile species in 103P/Hartley-2, supporting an interpretation of local mixing ratio variations, although the bulk average was homogeneous within uncertainties. Further studies are clearly needed to characterize possible bulk abundance variations within cometary nuclei.

5. Conclusion

If any one thing has been made clear by comet studies to date it is that comets are a compositionally diverse population. Some comets, classified as "organics-normal" in their composition, have abundances of key volatiles (relative to water) like C_2H_6, C_2H_2, HCN, and CH_3OH that cluster around mean values (being about 0.6, 0.2, 0.2, and 2%, respectively). Some comets, for example C/1999 S4 and 73P/Schwachmann-Wachmann 3, are systematically depleted in volatiles relative to water and such comets are denoted as "organics-poor" (Mumma et al. 2003). Likewise, C/2001 A2, 17P/Holmes, and C/2007 W1 (Boattini) are systematically enriched in organic molecules and are denoted as "organics-rich" (Magee-Sauer et al. 2008; Gibb et al. 2007; Dello Russo et al. 2007; Villanueva et al. 2011b). However, the number of comets sampled to date represents only a very small percentage of the overall Oort cloud and Kuiper Belt populations, and so may not be representative.

It should therefore not be surprising to find a comet that does not fit within the paradigm of "organics-normal", "organics-rich" and "organics-poor" comets, and Lulin is an example of such a comet. The abundances of some organic species in Lulin are similar to those observed in "organics-normal" Oort Cloud comets. C_2H_6, for example, has an abundance of ~0.6%, consistent with the "normal" value. CH_4, though more variable among comets than C_2H_6, is within the normal range for comets, being ~1.05% in Lulin.

Differences occur when considering other volatile species. For example, C_2H_2 has an abundance of ~0.06% in Lulin, much less than the typical 0.2%. The HCN abundance was 0.13%, somewhat less than the 0.2% typically observed, but within range of that expected for the "organics-depleted" comets. H_2CO is also quite depleted in comet Lulin, with an abundance of about 0.1%. This, and the significant depletion of CO (2.2%), stands in contrast to the enriched

abundance of CH_3OH (~3.6%), perhaps suggesting highly efficient hydrogenation on or within its pre-cometary grains (similarly for the high C_2H_6/C_2H_2 ratio observed in Lulin).

Due to the exceptionally large geocentric Doppler shift of comet Lulin, we were able to sample 9 transitions of CH_4. The R0, R1, R3, R4, R5 and Q1, Q2 transitions were observed on Jan 31 using two settings. Sampling quantum states that cover a wide range of lower state energies allowed us to determine an accurate rotational temperature of (67 K for CH_4) and a methane spin temperature consistent with statistical equilibrium (and a lower limit of $T_{spin} > 32$ K, at the 3-sigma confidence level). Similarly, the water spin temperature is consistent with statistical equilibrium, suggesting a relatively warm formation temperature for the bulk volatiles in Comet Lulin. However, we acknowledge that spin temperature can be interpreted as the formation temperature only under the assumption of no spin conversion upon sublimation or during its long residence time in the nucleus. The caveats to this interpretation will be discussed in a future paper. How measured volatile abundances in comets relate to formation environment is a subject of ongoing study.

ACKNOWLEDGEMENTS

ELG, BPB, and undergraduate student ES gratefully acknowledge support from NSF's Planetary Astronomy program (NSF 0807939). We also acknowledge support from NASA's Planetary Astronomy program for MJM, GLV and BPB (RTOPs 344-32-07, 08-PAST08-0034) and MAD (09-PAST09-0034; PI: MAD), NASA's Planetary Atmospheres program for MAD (09-PATM09-0080; PI: MAD), and NASA's Astrobiology Program through the NASA Astrobiology Institute (RTOP 344-53-51 to MJM). We are grateful for the assistance of Keck support astronomer Scott Dahm during the observations. Data presented herein were obtained at the W.

M. Keck Observatory, which is operated as a scientific partnership among the California Institute of Technology, the University of California, and the National Aeronautics and Space Administration. The Observatory was made possible by the generous financial support of the W. M. Keck Foundation. The authors recognize and acknowledge the very significant cultural role and reverence that the summit of Mauna Kea has always had within the indigenous Hawaiian community.

References

Agúndez, M., Cernicharo, J., Goicoechea, J. R. 2008, A&A, 483, 831

A'Hearn, M. F., Millis, R. C., Schleicher, D. O., Osip, D. J., Birch, P. V. 1995. Icarus, 118, 223

Aikawa, Y., & Herbst, E. 1999, ApJ, 526, 314

Blake, G. A., Qi, C., Hogerheijde, M. R., Gurwell, M. A., Muhleman, D. O. 1999, Nature, 6724, 213

Bockelée-Morvan, D., Gautier, D., Lis, D. C., et al. 1998, Icarus, 133, 147

Bodewits, D., Villanueva, G. L., Mumma, M. J., et al. 2011, ApJ, 141, 12

Bonev, B. P. 2005, Towards a chemical taxonomy of comets: Infrared spectroscopic methods for quantitative measurements of cometary water (With an independent chapter on Mars polar science). Ph.D. Thesis. http://astrobiology.gsfc.nasa.gov/Bonev_thesis.pdf.

Bonev, B.P., Mumma, M. J., Villanueva, G. L., et al. 2007, ApJL, 661, 97

Bonev, B. P., Mumma, M. J., Radeva, Y. L., DiSanti, M. A., Gibb, E. L., Villanueva, G. L., 2008a, ApJ, 680, 61

Bonev, B. P., Mumma, M. J., Kawakita, H., Kobayashi, H., Villanueva, G. L., 2008b, Icarus, 196, 241

Bonev, B. P., Mumma, M. J., Gibb, E. L., et al. 2009, ApJ, 699, 1563

Boogert, A. C. A., Pontoppidan, K. M., Knez, C. et al. 2008, ApJ, 678, 985

Boogert, A. C. A., Huard, T. L., Cook, A. M., et al. 2011, ApJ, 729, 92

Boudin, N., Schutte, W. A., & Greenberg, J. M. 1998, A&A, 331, 749

Chin, G., & Weaver, H. A. 1984, ApJ, 285, 858

Clough, S. A., Shephard, M. W., Mlawer, E. J., et al. 2005, J. Quant. Spectrosc. Radiat. Transfer, 91, 233

Combi, M. R., Delsemme, A. H. 1986, ApJ, 308, 472

Cook, A. M., Whittet, D. C. B., Shenoy, S. S., Gerakines, P. A., White, D. W., Chiar, J. E. 2011, ApJ, 730, 124

Cottin, H., & Fray, N. 2008, SSRv, 138, 179

Fray, N., Bénilan, Y., Cottin, H., Gazeau, M.-C., Crovisier, J. 20005, P&SS, 53, 1243

Crovisier, J. 2000, IAUS, 197, 461

Dello Russo, N., DiSanti, M. A., Mumma, M. J., Magee-Sauer, K., & Rettig, T. W. 1998, Icarus 135, 377

Dello Russo, N., Mumma, M. J., DiSanti, M. A., Magee-Sauer, K., Novak, R., & Rettig, T. W. 2000, Icarus 143, 324

Dello Russo, N., Disanti, M. A., Magee-Sauer, K., et al. 2004, Icarus 168, 186

Dello Russo, N., Bonev, B. P., DiSanti, M. A., et al. 2005, ApJ, 621, 537

Dello Russo, N., Vervack, R. J., Weaver, H. A., et al. 2007, Nature, 448, 172

Dello Russo, N., Vervack, Jr., R. J., Weaver, H. A., et al. 2009, ApJ, 703, 187

DiSanti, M. A., Mumma, M. J., Dello Russo, N., Magee-Sauer, K. 2001, Icarus, 153, 361.

DiSanti, M. A., Mumma, M. J., Dello Russo, N., Magee-Sauer, K., Griep, D. M. 2003, JGRE, 108, 5061

DiSanti, M. A., Bonev, B. P., Magee-Sauer, K., et al. 2006, ApJ, 650, 470

DiSanti, M. A., Villanueva, G. L., Bonev, B. P., et al. 2007, Icarus, 187, 240

DiSanti, M. A., Villanueva, G. L., Milam, S. N. et al. 2009, Icarus, 203, 589

Eberhardt, P., Reber, M., Krankowsky, D., Hodges, R. R. 1995, A&A, 302, 301

Fink, U., Combi, M. R., DiSanti, M. A., 1991, ApJ, 383, 356

Fink, U. 2009, Icarus, 201, 311

Fray, N., Bénilan, Y., Cottin, H., Gazeau, M.-C., & Crovisier, J. 2003, Planet. Space Sci., 53, 1243

Geiss, J., & Gloeckler, G. 1998, Sp. Sci. Rev., 84, 239

Gerakines, P. A., Whittet, D. C. B., Ehrenfreund, P., et al. 1999, ApJ, 522, 357

Gibb, E. L., Mumma, M. J., Dello Russo, N., DiSanti, M. A., Magee-Sauer, K. 2003, Icarus, 165, 391

Gibb, E. L., Whittet, D. C. B., Boogert, A. C. A., Tielens, A. G. G. M. 2004, ApJS, 151, 35

Gibb, E. L., DiSanti, M. A., Magee-Sauer, K., Dello Russo, N., Bonev, B. P., & Mumma. M. J. 2007, Icarus, 188, 224

Hartogh, P., Dariusz, C. L., Bockelée-Morvan, B., et al. 2011, Nature, 478, 218

Heinzeller, D., Nomura, H., Walsh, C., and Millar, T. J. 2011, ApJ, 731, 115.

Helbert, J., Rauer, H., Boice, D. C., Huebner, W. F. 2005, A&A, 442, 1007

Hoban, S., Mumma, M., Reuter, D. C., et al. 1991, Icarus, 93, 122

Hougen, J. T., & Oka, T. 2005, Science, 310, 1913

Huebner, W. F., Keady, J. J., and Lyon, S. P., 1992, ApSS, 195, 1

Kawakita, H. and M. J. Mumma 2011, ApJ, 727, 91

Kawakita, H., and Kobayashi, H. 2009, ApJ, 693, 388

Kawakita, H., Watanabe, J.-i., Furusho, R., Fuse, T., Capria, M. T., De Sanctis, M. C., Cremonese, G. 2006, ApJ, 601, 1152

Kawakita, H., Watanabe, J.-i., Furusho, R., Fuse, T., Boice, D. C. 2005, ApJL, 623, 49

Knight, M., Schleicher, D., 2009, IAUC, 9025, 1

Kobayashi, H., and Kawakita, H. 2009, ApJ, 703, 121

Kobayashi, H., Bockelée-Morvan, D., Kawakita, H., et al. 2010, A&A, 509, A80

Levison, H. F., Duncan, M. J., Brasser, R., Kaufmann, D. E., 2010, Science, 329, 187

Magee-Sauer, K., Mumma, M. J., DiSanti, M. A., Dello Russo, N., & Rettig, T. W. 1999, Icarus 142, 498

Magee-Sauer, K., Mumma, M. J., DiSanti, M. A., Dello Russo, N., 2002, JGRE, 107, 5096

Magee-Sauer, K., Mumma, M. J., DiSanti, M. A., et al. 2008, Icarus, 194, 347

McLean, I. S., & 14 coauthors. 1998, Proc. SPIE, 3354, 566

Meier, R., Owen, T. C., Matthews, H. E., et al. 1998, Science, 279, 842

Millar, T. J., Bennett, A., Herbst, E. 1989, ApJ, 340, 906

Mumma, M. J., & Charnley, S. B. 2011, ARA&A, 49, 471

Mumma, M. J., DiSanti, M. A., Dello Russo, N., Magee-Sauer, K., Gibb, E. L., & Novak, R., 2003, Adv. Sp. Res. 31 (No. 12), 2563

Mumma, M. J., Dello Russo, N., DiSanti, M. A., et al. 2001, Science, 292, 1334

Mumma, M. J., Weaver, H. A., Larson, H. P. 1987, A&A, 187, 419

Nakano, S. 2009, "C/2007 N3", Nakano Note NK 1834, Oriental Astron. Assn., http://www.Oaa.gr.jp/~oaacs/nk/nk1834.htm

Nummelin, A., Whittet, D. C. B., Gibb, E. L., Gerakines, P. A., and Chiar, J. E., 2001, ApJ, 558, 185

Öberg, K. I., van Broekhuizen, F., Fraser, H. J., et al. 2005, ApJ, 621, L33

Öberg, K. I., Boogert, A. C. A., Pontoppidan, K. M., et al. 2008, ApJ, 678, 1032

Pontoppidan, K. M., Dartois, E., van Dishoeck, E. F., Thi, W.-F., d'Hendecourt, L. 2003, A&A, 404, L17

Pontoppidan, K. M., Boogert, A. C. A., Fraser, H. J., et al. 2008, ApJ, 678, 1005

Radeva, Y. L., Mumma, M. J., Villanueva, G. L., A'Hearn, M. F. 2011, ApJ, 729, 135

Reuter, D. C., Hoban, S., & Mumma, M. J. 1992, Icarus, 95, 330

Sandford, S. A., & Allamandola, L. J. 1993, ApJ, 417, 815

Schleicher, D. G. 2008, AJ, 136, 2204

Stern, S. A. 2003, Nature, 424, 639

Tielens, A. G. G. M., & Allamandola, L. J. 1987, in Physical Processes in Interstellar clouds, ed. G. E. Morfill & M Schöler (Dordrecht: Reidel), 333

Villanueva, G. L., Mumma, M. J., Novak, R. E., Hewagama, T. 2008, Icarus, 195, 34

Villanueva, G. L., Mumma, M. J., Bonev, B. P., et al. 2009, ApJ, 690, L5

Villanueva, G.L., Mumma, M.J. & Magee-Sauer, K. 2011a, JGRE, 116, 08012

Villanueva, G.L., Mumma, M.J., DiSanti, M.A., Bonev, B.P., et al. 2011b, Icarus. 216, 227

Villanueva, G.L., DiSanti, M.A., Mumma, M.J., and Xu, L.-H. 2011c, ApJ, in press.

Villanueva, G.L., Magee-Sauer, K. & Mumma, M.J. 2011d, Journal of Quantitative Spectroscopy and Radiative Transfer. In preparation.

Villanueva, G.L., Mumma, M.J., Bonev, B.P., Novak, R.E., Barber, R.J. & DiSanti, M.A. 2012, Journal of Quantitative Spectroscopy and Radiative Transfer, 113, 202.

Walsh, C., Millar, T. J., and Nomura, H. 2010, ApJ, 722, 1607

Walsh, K. J., & Morbidelli, A. 2011, A&A, 526, 126

Weissman, P. R., Asphaug, E, & Lowry, S. C. 2004, In Comets II, eds. M. C. Festou, H. U. Keller, & H. A. Weaver [Tucson: The University of Arizona Press], 337

Whittet, D. C. B., Cook, A. M., Herbst, E., Chiar, J. E., & Shenoy, S. S. 2011, ApJ, 742, 28

Willacy, K., & Woods, P. M. 2009, ApJ, 703, 479

Young, J. 2007, MPC, 61391, 29

Figure Captions

Figure 1: (A) Spatial profiles for methane and dust in comet Lulin. The profile of CH_4 (black), and the continuum emission (red) are shown normalized to the central 3 pixels, for KL2, order 23. We find that the spatial profiles for emissions from volatiles (spectral lines) and continuum are similar for the molecules we sampled. (B) Q-curve for the CH_4 emission profile shown in (A). The Q-curve reaches a plateau with increasing distance from the nucleus. The nucleus centered Q is smaller than the plateau value due to seeing, pointing errors, comet drift, etc. and the ratio between the central 9x3 pixel box and the plateau is the scaling factor, Q-scale, determined for each spectrum.

Figure 2: Detections of HCN and other species in comet Lulin on 30 January 2009. The spectrum shown (KL2, order 25) is overlain with the sum of synthetic and telluric models (red, top panel). Below are the best-fit fluorescent emission models for HCN (orange), H_2O (green), OH (blue), NH_3 (aqua), NH_2 (olive), C_2H_2 (purple). At bottom is the residual (x2) spectrum after subtracting all identified emission lines. The 1-sigma error envelope is overplotted in green. The NH_3 model falls within the 1-sigma error envelope and thus NH_3 is not detected. The tick marks above the spectra at top and bottom indicate the expected positions of the two strongest NH_3 emission lines.

Figure 3. As for Figure 2 for 1 February. The two strongest NH_3 emission features are detected and are, indicated with teal tick marks above the spectra at top and bottom.

Figure 4: Detections of CO and H_2O in comet Lulin on 1 February. The spectrum shown (M-band, order 16) is overlain with the sum of synthetic and telluric models (red, top panel). Below are the best-fit fluorescent emission models for H_2O (blue) and CO (orange). At bottom is the residual spectrum after subtracting all identified emission lines. The 1-sigma error envelope is overplotted in green.

Figure 5: Detection of H_2CO and OH* in comet Lulin. We show the combined H_2CO spectrum (black) for 31 January (order 21, KL2 and KL3). Above is the best-fit H_2CO model (red) and below is the best-fit OH* model (blue). At the top, the frequency coverage of the KL2 and KL3 settings is indicated. Note the OH* lines in the KL2/KL3 overlap region, which were used for inter-setting calibration.

Figure 6: Detections of CH_3OH and OH* in comet Lulin on 1 February. The spectrum shown at top (KL1, order 22) is overlain with the sum of the telluric and best-fit synthetic CH_3OH ν_3 models (red). The telluric model is shown in blue and the OH* model in green. The ν_3 CH_3OH model is shown (bottom) fully resolved (olive) and convolved to the resolution of the measured spectrum (black).

Figure 7: Detections of C_2H_6, CH_4, CH_3OH, and OH* in comet Lulin on 1 February. The spectrum shown at top (KL1, order 23) is overlain with the sum of the telluric (blue). Spectrum for 1 Feb, order 23 (top) with the telluric model overplotted (blue). The best fit fluorescent models for C_2H_6 (red), OH* (olive), CH_4 (green) are shown below. At bottom is the residual

spectrum after subtracting all identified emission lines. The excess emission is due primarily to the ν_2 band of methanol.

Figure 8: A comparison of abundance ratios (% relative to water) for commonly measured volatiles among comets. All abundances are relative to the cometary mean (see Villanueva et al. 2011b). Squares represent comet C/2001 A2 (Magee-Sauer et al. 2008), the comet defining "organics-rich". A similarly enriched comet (C/2007 W1 Boattini) is shown by diamonds (Villanueva et al. 2011b). Comet C/1999 S4 (blue asterisks; Mumma et al. 2001) represents the most systematically organics depleted comet observed to date. These comets define the current approximate range of abundances for most species (CO excepted). Red triangles connected by a red line show the abundances for Lulin. Note the more extreme variation from "enhanced" to "depleted" abundances for molecules in Lulin compared to the consistently "enhanced" or "depleted" comets.

Figure 9: A plot of total production rate over time for H_2O (black plus, divided by 100 for clarity), CH_4 (green diamonds), C_2H_6 (aqua triangles), HCN (red asterisks, multiplied by 2 for clarity), C_2H_2 (blue circles), H_2CO (purple squares, multiplied by two for clarity) and CO (teal cross) in Lulin illustrating the changes in overall production rates, in particular the dramatic increase on 1 Feb. All values are normalized to the Jan 31 water production rate. Note also, the changes in relative abundance of, for example, CH_4 over the three nights. The time increments over which the observations were taken are indicated with vertical dashed lines.

Figure 10: Detections of ortho-H_2O, para-H_2O, and OH* in comet Lulin on 31 January. The spectrum shown (KL2, order 26) is overlain with the sum of the telluric and best-fit synthetic fluorescent emission models (red, top panel). Below are the best-fit fluorescent emission model for ortho water (orange) and para water (purple). OH* prompt emission lines are indicated in blue. At bottom is the residual spectrum after subtracting all identified emission lines. The 1-sigma error envelope is overplotted in green. The best fit is for an OPR = 3:1 (statistical equilibrium).

Figure 11: Detection of CH_4 and OH* in comet Lulin on 31 January. The combined spectrum (KL2 and KL3, order 23) is overlain with the sum of the telluric and best-fit synthetic fluorescent emission model (red, top panel). At middle are shown fluorescence models for the three spin components of CH_4 (A: orange, E: purple, F: blue), and for OH prompt emission lines near 3040-3050 cm^{-1} (olive). At bottom is the residual with the best fit models subtracted (scaled by a factor of 2). The 1-sigma error envelope is overplotted in green, illustrating the exceptional quality of the fits. The best fit is for statistical equilibrium (A:E:F 5:3:2, T_{rot} >60 K).

Figure 12: As for Figure 10 for 30 January. At middle, the best fit fluorescent emission model for CH_4 (orange), OH* prompt emission near 3040-3050 cm^{-1} (blue), and CH_3D (purple) are shown. We performed a sensitive search for CH_3D but did not detect it. The sum of the telluric and best fit models (CH_4 + OH) is shown in red (top) and the residual (after subtracting the best-fit model) is shown at bottom (scaled by a factor of 2). The 1-sigma error envelope is overplotted in green, illustrating the excellent match between observation and model.

TABLE 1
OBSERVING LOG AND H_2O PRODUCTION RATES

UT date	NIRSPEC Setting	*UT*	R_h [AU]	$\Delta R_h/dt$ [km s^{-1}]	Δ [AU]	$d\Delta/dt$ [km s^{-1}]	T_{int} [min]	$Q(H_2O)$ (10^{29} s^{-1})
30 Jan 2009	KL2	13:48-15:01	1.251	6.7	0.985	-54.2	22	1.35(0.03)
	KL3	15:08-16:36	1.252	6.7	0.982	-54.1	8	
31 Jan 2009	KL2	13:23-14:25	1.255	7.0	0.955	-54.3	28	1.13(0.02)
	KL3	14:39-16:49	1.256	7.0	0.952	–54.1	36	
01 Feb 2009	KL1	13:44-14:54	1.256	7.3	0.923	-54.1	26	1.68(0.05)
	MWA	15:05-15:49	1.257	7.3	0.922	-54.1	12	2.01(0.05)
	MWC	15:56-16:35	1.258	7.3	0.921	-54.0	8	2.30(0.08)
	KL2	16:39-16:50	1.260	7.3	0.920	-53.9	8	2.68(0.11)

NOTE. – R_h, $\Delta R_h/dt$, Δ, and $d\Delta/dt$ are respectively heliocentric distance, heliocentric velocity, geocentric distance, and topocentric line-of-sight velocity of C/2007 N3; T_{int} is total integration time on source, and $Q(H_2O)$ is the water production rate, as described in §3

TABLE 2A
VOLATILE COMPOSITION OF COMET C/2007 N3 (LULIN)

Molecule	T_{rot} [a] [K]	Q [b, c] (10^{26} s^{-1})	Mixing Ratio [c] [%]
2009 Jan 30, R_h = 1.251 AU, Δ = 0.98 AU			
H_2O	68±2	1351±30	100
HCN	63±3	2.27±0.07	0.168±0.006
	(68)	2.33±0.08	0.172±0.007
NH_3	(68)	<2.5	<0.19
C_2H_2	(68)	1.12±0.09	0.083±0.007
CH_4	65±1	17.9±0.3	1.32±0.04
	(68)	18.8±0.4	1.39±0.04
CH_3D	(65)	<0.53	<0.039 [CH_3D/CH_4 < 2.9%]
C_2H_6 ν_5	72±8	9.30±0.48	0.69±0.04
	(68)	8.94±0.47	0.66±0.04
H_2CO	(68)	1.64±0.19 [d]	0.12±0.01 [d]
		1.82±0.48	0.13±0.04
2009 Jan 31, R_h = 1.255 AU, Δ = 0.95 AU			
H_2O	67±2	1130±20	100
HCN	72±6	1.44±0.08	0.127±0.007
	(67)	1.40±0.08	0.124±0.007
NH_3	(67)	<2.9	<0.22
C_2H_2	(67)	0.75±0.12	0.066±0.011
CH_4	68±2	13.5±0.4	1.19±0.04
CH_3D	(68)	<0.40	<0.035 [CH_3D/CH_4 < 2.9%]
C_2H_6 ν_5	74±8	7.51±0.50	0.664±0.046
	(67)	7.06±0.49	0.624±0.045
H_2CO	(67)	1.24±0.19[d]	0.11±0.02 [d]
		3.25±0.42	0.26±0.04
2009 Feb 1, R_h = 1.256 AU, Δ = 0.92 AU			
		KL1	
H_2O	69±1	1565±28	100
CH_4	(70)	17.4±0.4	1.11±0.03
C_2H_6 ν_7	(70)	13.5±0.4	0.86±0.03
CH_3OH ν_3	65±10	56.0±0.5	3.58±0.07
	(70)	56.7±0.5	3.62±0.07
		M-Wide A	
H_2O[e]	71±2	2013±50	100
CO[e]	(71)	43.60±1.58	2.17±0.10
		M-Wide C	

H_2O[e]	71±8	2300±80	100
CO[e]	(71)	52.85±3.4	2.30±0.17
		KL2	
H_2O	72±5	2477±79	100
HCN	63±3	2.52±0.06	0.102±0.004
	(70)	2.63±0.06	0.106±0.004
NH_3	(70)	6.83±1.38	0.28±0.06
C_2H_2	(70)	1.32±0.15	0.053±0.006
CH_4	(70)	23.5±1.8	0.949±0.08
C_2H_6 ν_5	(70)	12.8±0.3	0.52±0.02
H_2CO	(70)	2.62±0.36[d]	0.106±0.015[d]
		4.64±0.57	0.187±0.024

[a] Rotational temperature. Values in parentheses are assumed.

[b] Errors in production rate include both photon noise and line-by-line deviation between modeled and observed intensities (see Bonev et al. 2007, Dello Russo et al. 2004, Bonev 2005).

[c] Upper limits are 3σ.

[d] First values are for all lines included. The 2nd row is for the Q-branch only.

[e] The formal rotational temperature for CO was found to be 72±2 K, by combining all lines from both MWC/o17 and MWA/o16 (as shown in Fig. 4). Separate analysis of each order did not yield meaningful values for T_{rot} due to insufficient sampling of rotational energies.

TABLE 2b

WEIGHTED MEAN MIXING RATIOS (X/H_2O [%]) FOR INDIVIDUAL SPECIES[A]

Comet	HCN	C_2H_2	CH_4	C_2H_6	CO	H_2CO	CH_3OH	NH_3
C/2007 N3 (Lulin	0.13±0.01	0.07±0.03	1.02±0.30	0.63±0.14	2.26±0.20	0.11±0.05	3.58±0.07	0.28±0.06
C/2001 A2	0.6±0.1	0.5±0.1	1.6±0.2	1.7±0.2	3.9±1.1	0.06±0.03	3.9±0.4	-
C/1999 S4	0.10±0.03	<0.12 (3σ)	0.18±0.06	0.11±0.02	0.9±0.3	-	<0.15	-
C/2007 W1 (Boatt	0.50±0.01	0.29±0.02	1.57±0.16	1.96±0.04	4.50±0.51	<0.12 (3σ)	3.87±0.09	1.74±0.17

[a] Abundances from: Lulin – weighted averages of all measurements in Table 2a in this work, C/2001 A2 (H_2CO and CH_4 from Gibb et al. 2007, remaining molecules from Magee-Sauer et al. 2008), C/1999 S4 (Mumma et al. 2001), C/2007 W1 Boattini (Villanueva et al. 2011b, not assuming enhanced polar abundances. See section 3.2 for caveats.)

TABLE 3
Comparison of Primary and Putative Product species in C/2007 N3 (Lulin)

$\log_{10}$ [Q(CN)/Q(OH)]	$\log_{10}$ [$Q(C_2)/Q(OH)$]	$\log_{10}$ [$Q(C_2)/Q(CN)$]	
-2.76,-2.80	-2.33,-2.36	0.431,0.436	
$\log_{10}$ [$Q(HCN)/Q(H_2O)$]	$\log_{10}$ [$Q(C_2H_2)/Q(H_2O)$]	$\log_{10}$ [$Q(C_2H_2)/Q(HCN)$]	$\log_{10}$ [$Q(C_2H_2+0.5*C_2H_6)/Q(HCN)$]
-2.90	-3.20	-0.298	0.485

Note: CN, OH, and C_2 production rates are from Bodewits et al. (2011). The remaining production rates are from this work. See section 4.2 for caveats concerning the possible release of product C_2 from an ethane parent.

TABLE 4. OBSERVED EMISSION LINES AND RELEVANT PARAMETERS

TABLE 4A. OBSERVED EMISSION LINES AND RELEVANT PARAMETERS FOR HYDROCARBON SPECIES

Transition	**Frequency [cm^{-1}]**	**Flux[a] 10^{-20} [$W\ m^{-2}$]**	**Sigma flux 10^{-20} [$W\ m^{-2}$]**	**E_{rot} [cm^{-1}]**	**g-factor [s^{-1}]**	**Atmospheric transmittance**
Jan 30, ν_3-band of CH_4 at 67 K (Villanueva et al., in prep)– gfactors x 10^{-6}						
Q-branch	3019.18	195.85	3.70	32.22	61.6	0.38
R0	3029.21	132.28	1.92	0.00	26.9	0.81
R1	3039.00	130.21	1.58	10.48	21.9	0.85
R3	3058.31	243.77	4.55	62.88	48.8	0.61
R4	3067.87	140.80	4.72	104.77	22.5	0.56
R5	3077.26	60.90	4.54	157.13	7.07	0.62
Jan 31, ν_3-band of CH_4 at 67 K– gfactors x 10^{-6}						
Q-branch	3019.29	172.31	3.33	30.93	52.4	0.39
R0	3029.34	160.41	2.05	0.00	27.5	0.78
R1	3039.07	154.51	1.34	10.48	22.3	0.85
R3	3058.33	244.22	2.63	62.88	48.9	0.59
R4	3067.86	137.85	2.81	104.78	28.9	0.49
R5	3077.25	64.80	3.02	157.13	94.9	0.56
Feb 01, ν_3-band of CH_4 at 70 K– gfactors x 10^{-6}						
Q-branch	3019.2419	233.35	3.09	30.93	50.8	0.54
R0	3029.3397	251.28	3.26	0.00	25.8	0.88
R1	3039.0714	422.91	5.99	10.48	21.1	0.90
P2	2999.6100	169.72	1.86	31.44	12.9	0.90
P3	2989.3200	85.91	2.27	62.88	11.1	0.59
P4	2979.3900	149.81	3.32	104.77	16.9	0.59
P5	2969.4000	81.94	2.20	157.13	3.37	0.79
Transition	**Frequency [cm^{-1}]**	**Flux 10^{-20} [$W\ m^{-2}$]**	**Sigma flux 10^{-20} [$W\ m^{-2}$]**	**E_{rot} [cm^{-1}]**	**g-factor [s^{-1}]**	**Atmospheric transmittance**
Jan 30, ν_5-band of C_2H_6 at 55 K (Villanueva et al. 2011a)– gfactors x 10^{-5}						
R4	2903.27	28.58	2.04	22.34	0.61	0.99
R3	2901.77	12.95	2.50	13.49	0.54	0.84
Q	2896.08	57.82	5.23	68.79	2.11	0.67
P2	2892.32	110.75	1.94	10.58	0.35	0.98
P3	2891.06	11.60	2.10	19.16	0.46	0.97
P5	2889.84	23.70	2.10	25.75	0.67	0.99
P6	2888.62	24.61	2.36	34.95	0.65	0.87
P7	2887.53	33.28	2.36	45.79	0.85	0.96
P8	2886.40	22.39	2.37	59.55	0.77	0.95
P9	2884.26	12.52	2.62	78.26	0.55	0.75
Jan 31, ν_5-band of C_2H_6 at 67 K– gfactors x 10^{-5}						
R4	2903.23	19.35	2.17	20.03	0.58	0.99
R3	2901.73	10.33	2.73	13.49	0.54	0.84
Q	2896.05	29.96	5.64	66.86	2.09	0.66

P2	2892.29	7.05	2.07	10.58	0.35	0.98
P3	2891.03	10.61	2.25	19.16	0.46	0.98
P5	2889.81	20.28	2.27	25.75	0.67	0.99
P6	2888.64	13.47	2.55	34.95	0.65	0.87
P7	2887.51	27.83	2.59	45.80	0.85	0.96
P8	2886.37	20.78	2.46	59.55	0.71	0.95
P9	2884.23	11.83	2.65	76.84	0.41	0.91
Feb 01, ν_7-band of C_2H_6 at 70 K– gfactors x 10^{-5}						
$^{R}Q_4$	3000.72	126.5	2.42	86.44	1.56	0.97
$^{R}Q_2$	2994.00	192.8	2.26	65.61	2.63	0.88
$^{R}Q_1$	2990.59	256.1	2.10	55.63	3.24	0.96
$^{R}Q_0$	2987.28	295.0	3.06	49.82	4.23	0.77
$^{P}Q_1$	2983.91	235.1	2.14	51.27	3.24	0.92
$^{P}Q_2$	2980.58	206.2	2.88	60.04	2.67	0.89

[a] The listed flux is the value after correction for atmospheric transmittance. Transmittance values are given in column 6. See also discussion in section 2.

TABLE 4B. OBSERVED EMISSION LINES AND RELEVANT PARAMETERS FOR NITROGEN BEARING SPECIES

Transition	**Frequency [cm^{-1}]**	**Flux[a] 10^{-20} [W m^{-2}]**	**Sigma flux 10^{-20} [W m^{-2}]**	**E_{rot} [cm^{-1}]**	**g-factor [s^{-1}]**	**Atmospheric transmittance**
Jan 30, ν_1-band of HCN at 55 K (Villanueva et al. 2011d)– gfactors x 10^{-5}						
R1	3317.92	18.25	1.21	2.96	1.99	0.96
R0	3315.00	8.23	1.16	0.00	1.15	0.86
P2	3306.11	27.60	1.32	8.87	2.30	0.97
P3	3303.18	24.61	1.86	17.74	3.00	0.46
P5	3297.09	26.56	1.71	44.34	3.03	0.71
P6	3294.07	24.32	1.82	62.08	2.54	0.59
P7	3290.95	18.50	1.46	82.77	1.93	0.82
P8	3287.82	13.46	1.23	106.41	1.33	0.91
P9	3284.78	10.55	1.18	133.02	0.85	0.96
P10	3281.64	3.13	1.18	162.57	0.49	0.96
Jan 31, ν_1-band of HCN at 63 K– gfactors x 10^{-5}						
R1	3317.98	12.64	0.99	2.96	1.80	0.92
R0	3314.96	2.87	1.17	0.00	1.02	0.71
P2	3306.20	12.77	1.10	8.87	2.05	0.95
P3	3303.17	12.94	2.10	17.74	2.71	0.33
P5	3297.12	19.47	1.61	44.34	2.91	0.56
P6	3294.06	8.94	1.70	62.08	2.55	0.37
P7	3291.00	14.11	1.58	82.77	2.03	0.69
P8	3287.87	12.07	1.38	106.41	1.49	0.83
P9	3284.74	8.73	1.43	133.01	1.01	0.92
P10	3281.65	5.89	1.30	162.57	0.64	0.93
Feb 01, ν_1-band of HCN at 70 K– gfactors x 10^{-5}						
R1	3317.89	43.26	2.03	2.96	2.96	0.97

R0	3315.05	15.81	1.77	0.00	0.00	0.88
P2	3306.13	38.78	2.03	8.87	8.87	0.98
P3	3303.14	31.64	2.89	17.74	17.74	0.65
P4	3300.10	60.89	2.53	29.56	29.56	0.80
P5	3297.09	44.51	2.93	44.34	44.34	0.80
P6	3294.02	35.76	2.51	62.08	62.08	.69
P7	3290.95	31.75	2.03	82.77	82.77	0.87
P8	3287.82	28.73	1.87	106.42	106.42	0.93
P9	3284.73	31.07	2.15	133.02	133.02	0.97
P10	3281.58	15.90	1.82	162.57	162.57	0.97
P11	3278.42	11.30	1.98	195.07	195.07	0.92
P12	3275.25	7.75	2.41	230.53	230.53	0.63
Feb 01, ν_1-band of NH_3 at 70 K (Villanueva et al. 2011d)– gfactors x 10^{-5}						
aP(2,0), aP(2,1)	3295.97	14.25	2.19	59.61	0.24	0.95
sqP(3,0),sqP(3,1)	3277.58	20.92	2.75	116.25	0.27	0.92

[a] The listed flux is the value after correction for atmospheric transmittance. Transmittance values are given in column 6. See also discussion in section 2.

TABLE 4C. OBSERVED EMISSION LINES AND RELEVANT PARAMETERS FOR OXYGEN BEARING SPECIES

Transition	**Frequency [cm^{-1}]**	**Flux[a] 10^{-20} [W m^{-2}]**	**Sigma flux 10^{-20} [W m^{-2}]**	**E_{rot} [cm^{-1}]**	**g-factor [s^{-1}]**	**Atmospheric transmittance**
Jan 30, ν_1-band of H_2CO at 70 K (DiSanti et al. 2006)– gfactors x 10^{-5}						
Q-branch	2781.55	11.24	1.92	101.10	1.16	0.98
Jan 31, ν_1-band of H_2CO at 70 K– gfactors x 10^{-5}						
Q-branch	2781.53	16.73	2.67	104.96	1.22	0.96
Feb 1, ν_1-band of H_2CO at 70 K– gfactors x 10^{-5}						
Q-branch	2781.55	50.06	8.54	106.21	1.04	0.98
Feb 1, ν_3-band of CH_3OH at 70 K (Villanueva et al. 2011c)– gfactors x 10^{-5}						
Q-branch	2844.81	470.23	4.46	84.56	1.53	0.98
Feb 1, ν_1-band of CO at 72 K (Villanueva et al. 2011b)– gfactors x 10^{-6}						
R10	2183.2239	33.94	23.05	251.36	0.921	0.75
R9	2179.7720	104.6	19.96	209.48	1.87	0.80
R8	2176.2834	76.38	16.29	171.40	3.43	0.90
R7	2172.7588	119.6	15.84	137.13	5.76	0.92
R6	2169.1980	225.4	18.30	106.66	8.67	0.85
R5	2165.6011	268.0	13.45	80.00	12.3	0.93
R3	2158.2998	243.9	12.47	38.10	14.1	0.84
R2	2154.5955	370.5	10.92	22.86	17.6	0.94
R1	2150.0856	313.0	11.47	11.43	12.5	0.93
R0	2147.0811	172.1	15.42	3.81	8.26	0.84
P1	2139.4260	123.8	12.17	0.00	6.38	0.87
P2	2135.5461	375.6	12.86	3.81	16.2	0.90
P3	2131.6316	388.5	12.03	11.80	18.5	0.83

P4	2127.6824	437.7	10.88	22.86	22.6	0.91

Transition	Frequency [cm^{-1}]	Flux[a] 10^{-20} [W m^{-2}]	Sigma flux 10^{-20} [W m^{-2}]	E_{rot} [cm^{-1}]	g-factor [s^{-1}]	Atmospheric transmittance
Jan 31, H_2O at 67 K (Villanueva et al., 2012)– gfactors x 10^{-9}						
O $(101)3_{13}$-$(100)3_{30}$	3450.90	5.01	1.09	180.34	6.49	0.90
P $(201)2_{12}$-$(200)1_{11}$	3450.82				4.95	
P $(200)5_{15}$-$(100)5_{24}$	3450.78				0.31	
O $(200)1_{10}$-$(001)1_{11}$	3450.29	98.28	1.13	36.41	140.82	0.88
O $(100)3_{30}$-$(000)4_{41}$	3447.24	312.4	11.32	486.88	349.6	0.14
P $(100)3_{31}$-$(000)4_{40}$	3447.08				97.28	
O $(200)2_{21}$-$(001)2_{20}$	3442.31	106.23	14.09	131.19	175.93	0.12
P $(001)4_{23}$-$(000)5_{42}$	3439.94	38.59	3.70	54.33	0.78	0.39
P $(200)1_{11}$-$(001)1_{10}$	3439.83				61.74	
O $(200)4_{23}$-$(100)5_{14}$	3439.82				1.14	
P $(120)2_{20}$-$(020)3_{31}$	3435.57	12.49	1.65	231.73	0.29	0.74
P $(220)3_{22}$-$(001)3_{21}$	3435.49				10.34	
O $(210)1_{10}$-$(011)1_{11}$	3435.40				0.49	
O $(111)4_{22}$-$(110)5_{23}$	3435.34				2.93	
P $(101)2_{12}$-$(001)3_{03}$	3434.40	27.73	1.10	172.86	22.21	0.94
P $(101)4_{14}$-$(100)4_{31}$	3434.38				0.98	
O $(120)2_{21}$-$(020)3_{30}$	3434.38				0.81	
P $(200)2_{11}$-$(100)3_{22}$	3434.33				17.14	
O $(100)4_{14}$-$(000)5_{23}$	3431.06	74.73	1.68	446.51	105.88	0.72
O $(200)2_{12}$-$(001)2_{11}$	3428.30	38.28	1.18	95.33	57.18	0.88
P $(101)6_{25}$-$(100)7_{26}$	3427.99	11.56	1.24	650.27	0.37	0.82
O $(001)5_{15}$-$(000)6_{34}$	3427.92				13.77	
O $(101)2_{02}$-$(001)3_{13}$	3422.33	50.50	1.98	139.66	84.35	0.69
P $(200)5_{15}$-$(100)6_{06}$	3420.60	54.63	4.80	60754	1.40	0.34
O $(100)4_{32}$-$(000)5_{41}$	3420.50				0.82	
P $(201)1_{10}$-$(200)1_{11}$	3415.80	16.41	1.18	218.83	7.70	0.94
P $(101)3_{03}$-$(100)4_{22}$	3415.73				0.16	
P $(201)3_{21}$-$(200)3_{22}$	3413.08	46.09	1.37	218.90	0.67	0.82
O $(001)6_{06}$-$(000)7_{25}$	3413.07				1.28	
O $(200)2_{12}$-$(100)3_{21}$	3412.92				70.18	
O $(101)3_{13}$-$(001)4_{04}$	3411.62	32.31	1.13	218.36	49.58	0.93
O $(201)2_{20}$-$(200)2_{21}$	3409.05	50.32	1.53	396.97	7.73	0.93
O $(110)3_{30}$-$(010)4_{41}$	3409.05				20.07	
O $(100)3_{03}$-$(000)4_{32}$	3408.86				47.38	
O $(201)1_{11}$-$(200)1_{10}$	3405.42	26.85	0.99	49.50	26.15	0.96
P $(201)2_{21}$-$(200)2_{20}$	3405.39				24.10	
P $(101)3_{03}$-$(001)4_{14}$	3405.03	9.29	1.06	221.33	11.88	0.96
P $(101)1_{10}$-$(001)2_{21}$	3404.24	16.84	1.15	129.81	25.02	0.93
O $(110)4_{14}$-$(010)5_{23}$	3403.40	41.52	6.97	103.17	1.81	

P $(200)1_{11}$-$(001)2_{12}$	3403.23				63.68	0.26

[a] The listed flux is the value after correction for atmospheric transmittance. Transmittance values are given in column 6. See also discussion in section 2.

Figure 1:

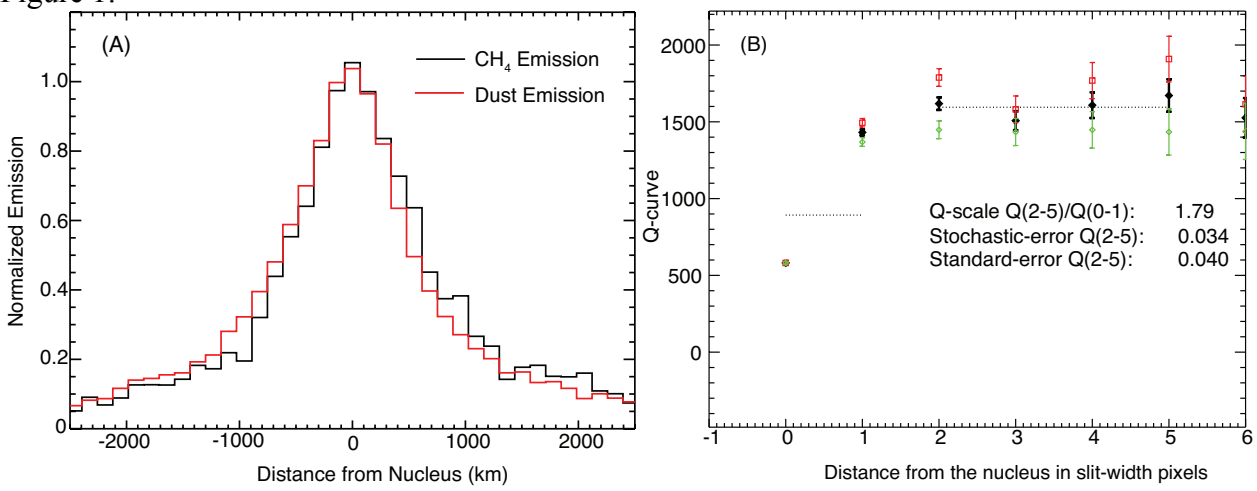

Figure 2:

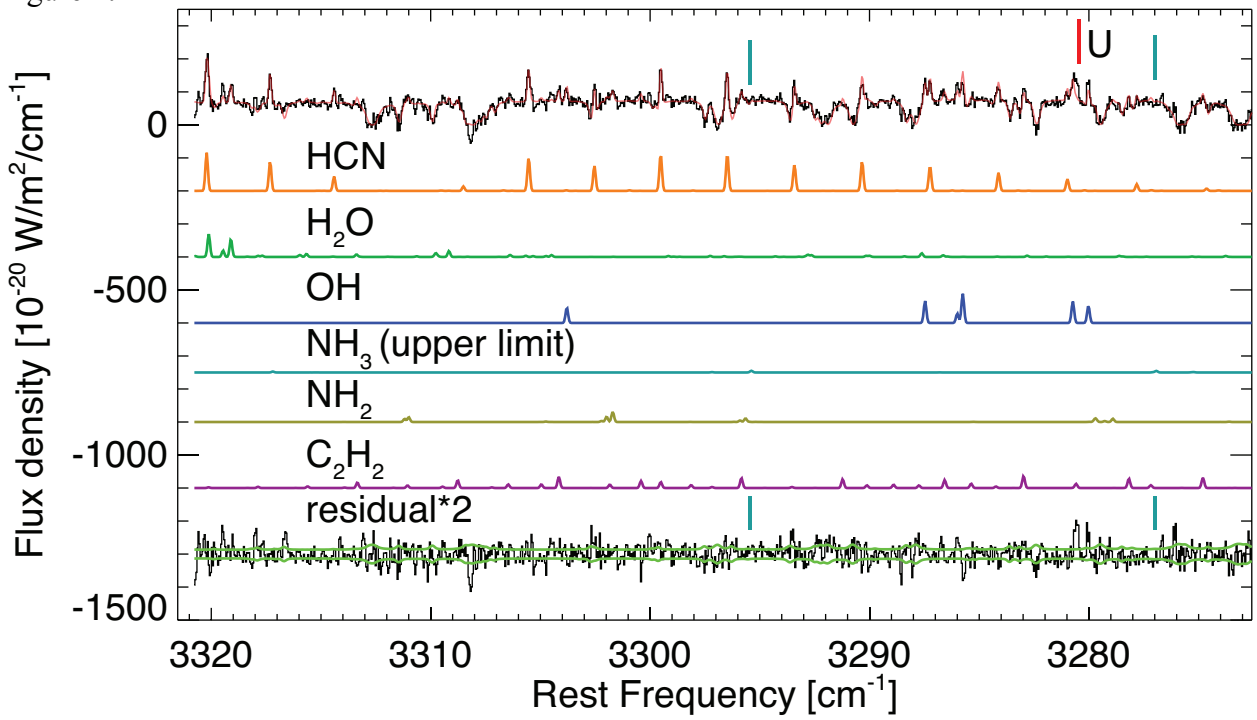

Figure 3:

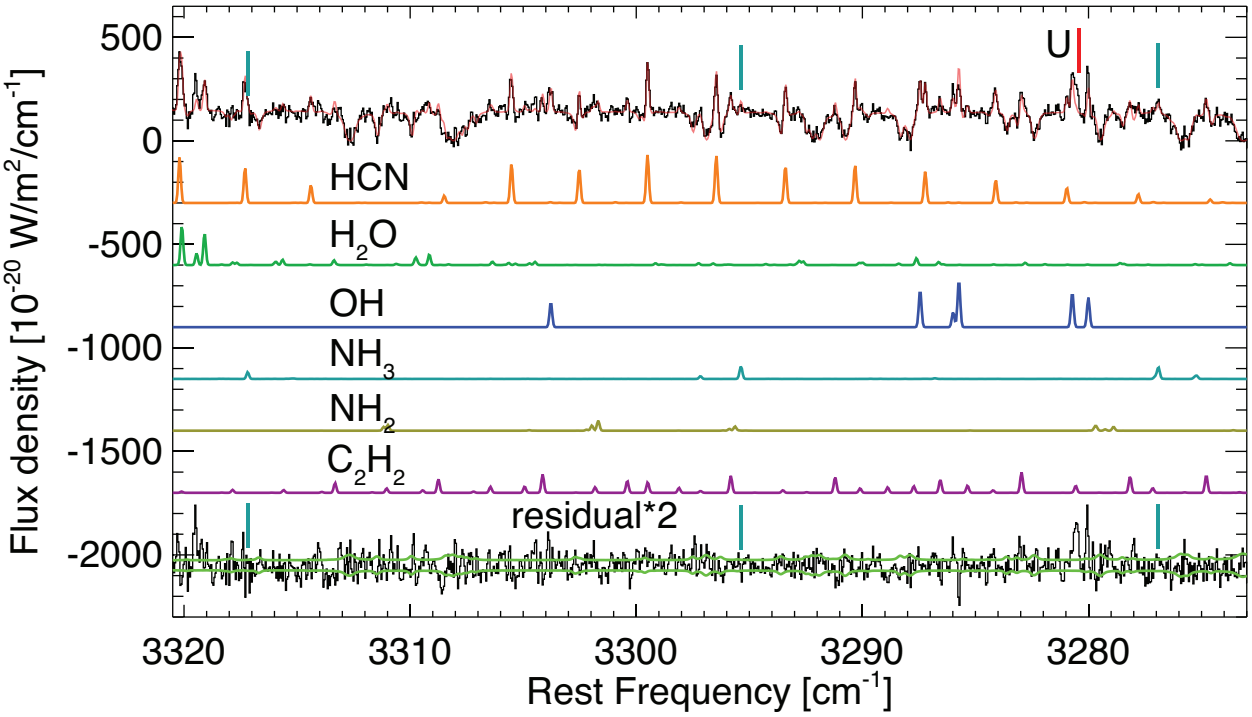

Figure 4:

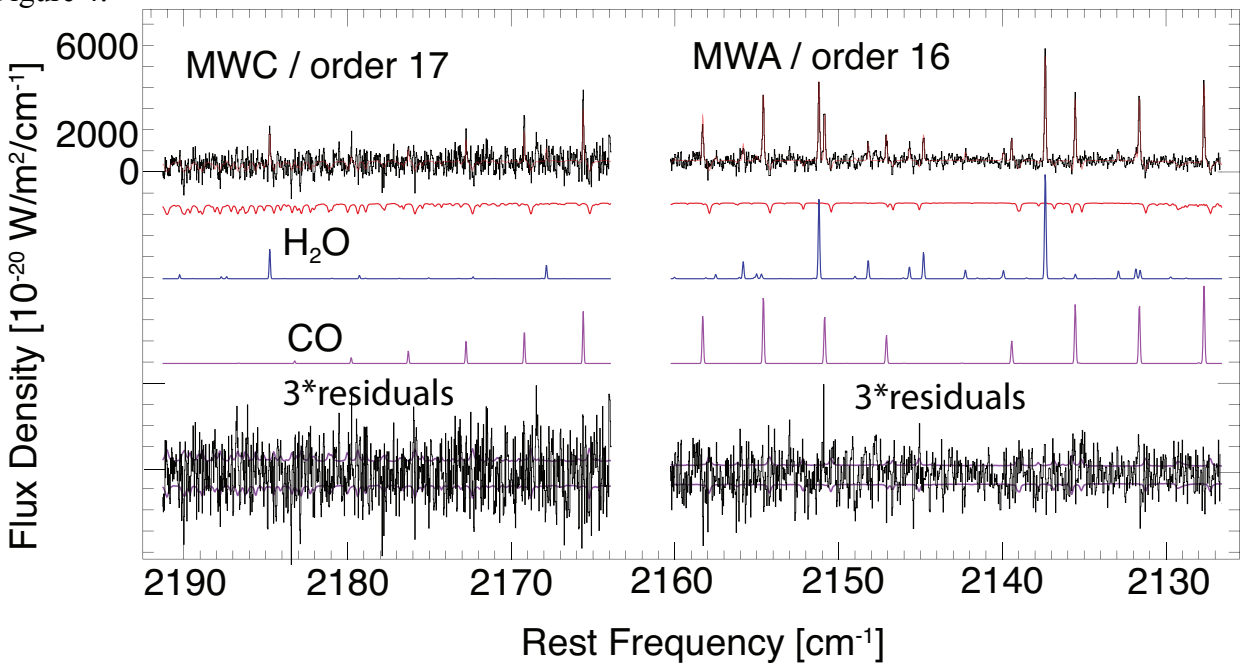

Figure 5:

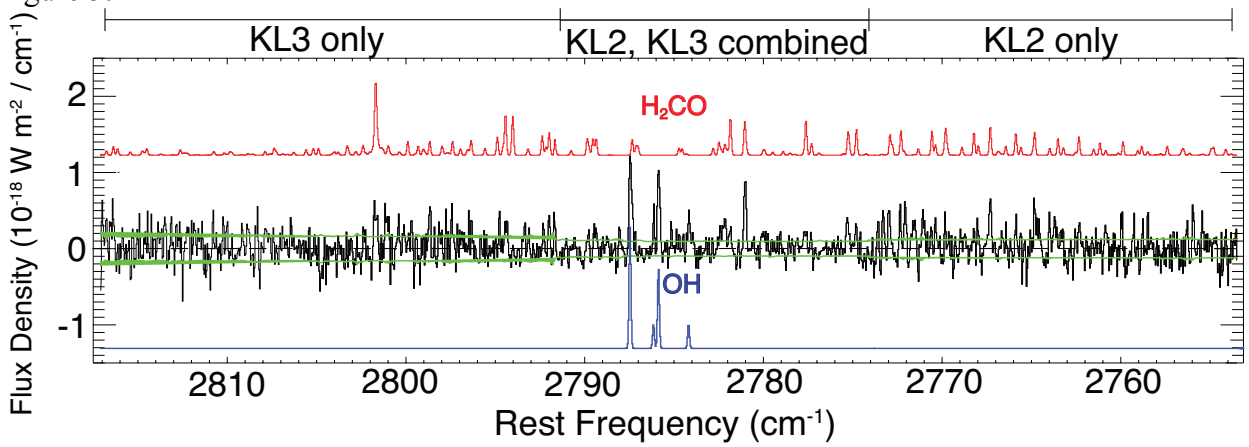

Figure 6:

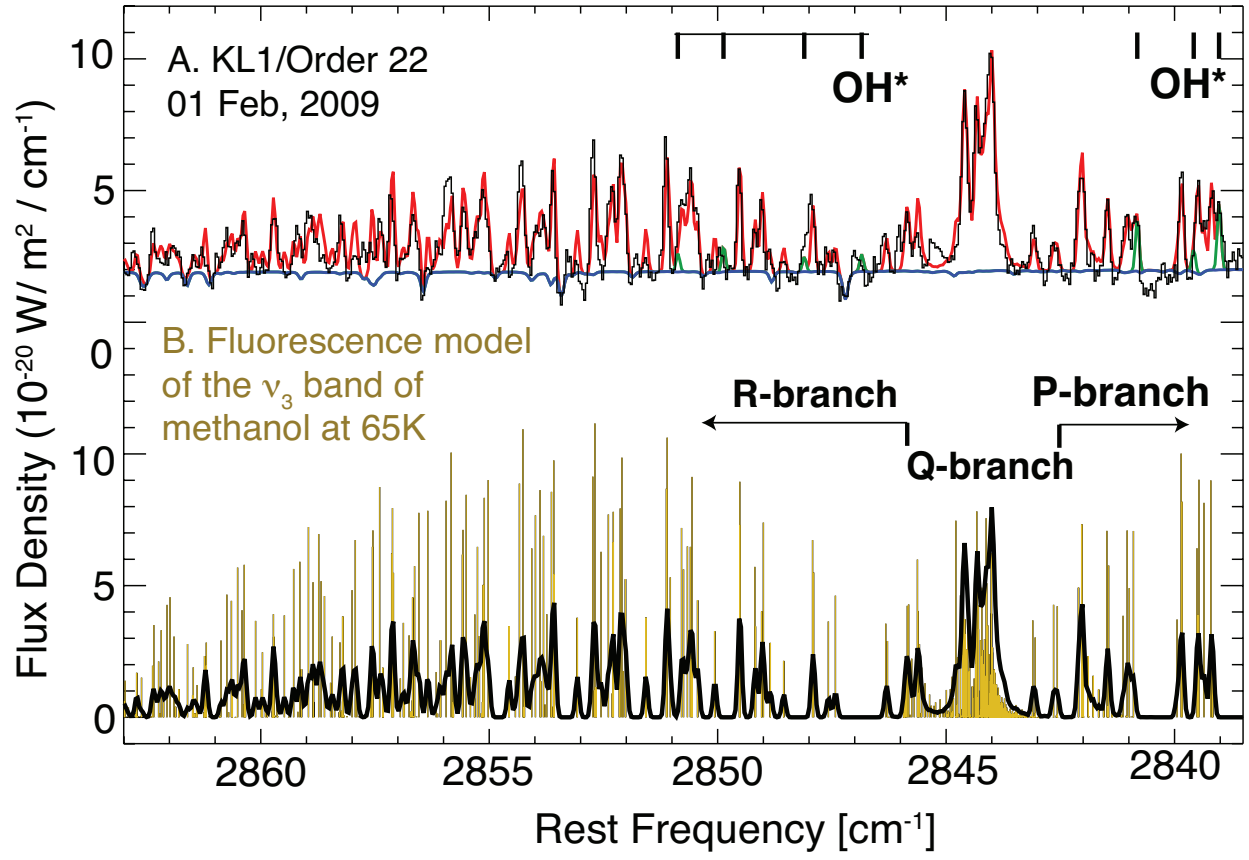

Figure 7:

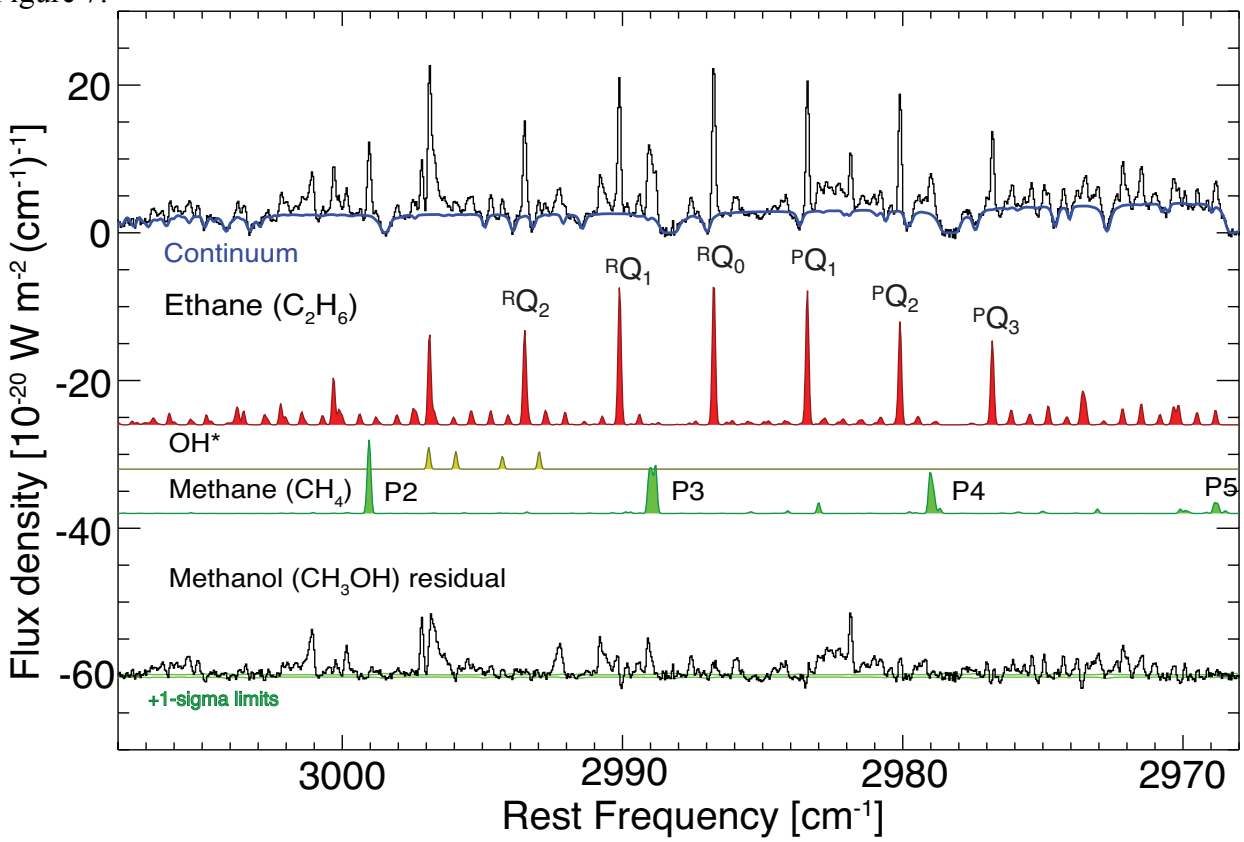

Figure 8:

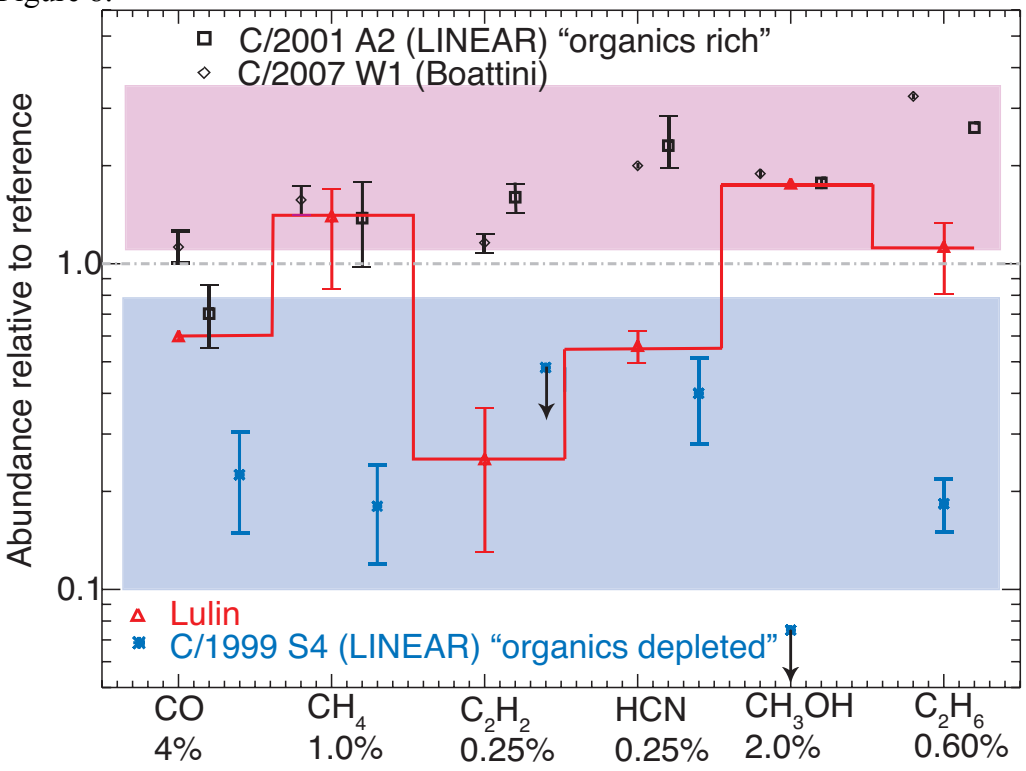

Figure 9:

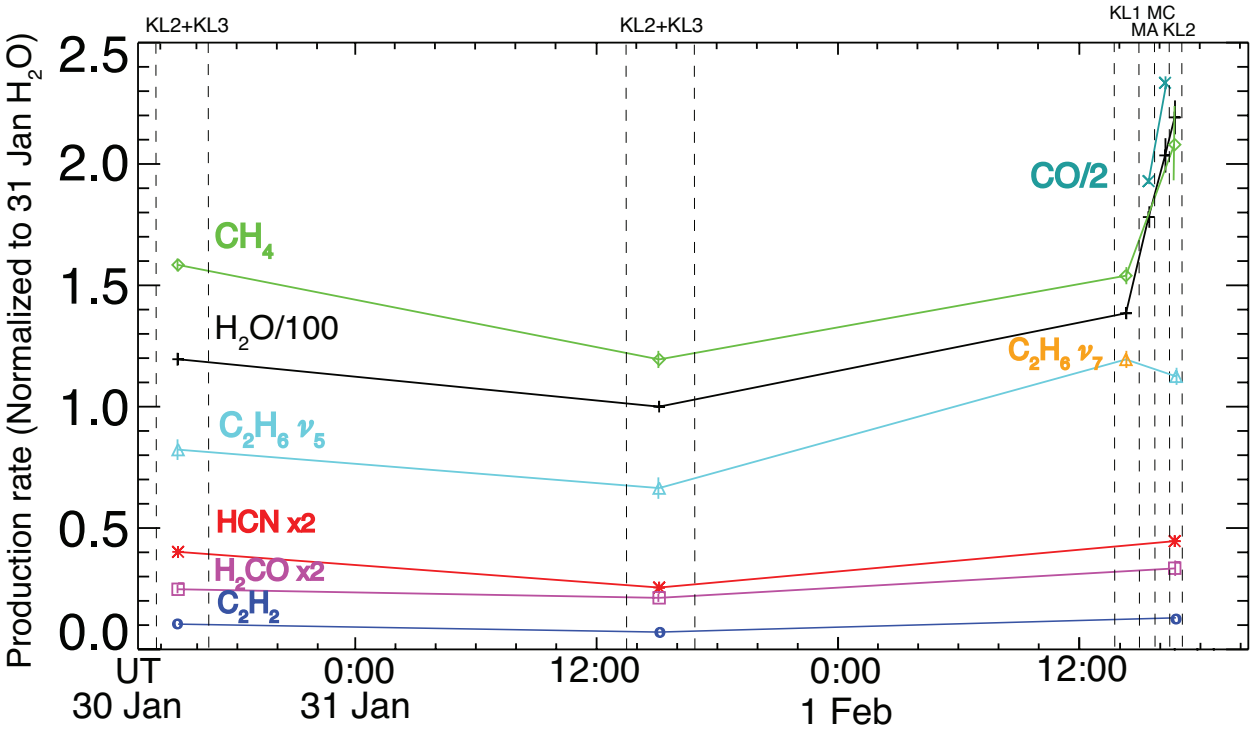

Figure 10:

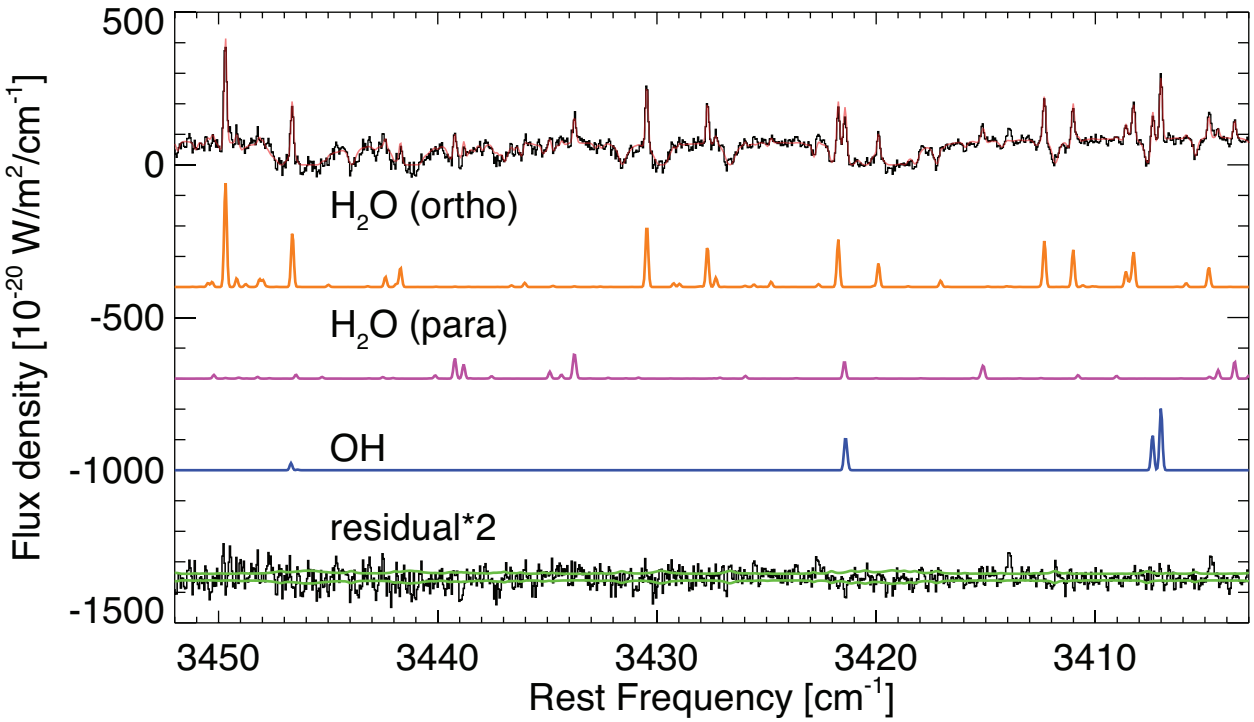

Figure 11:

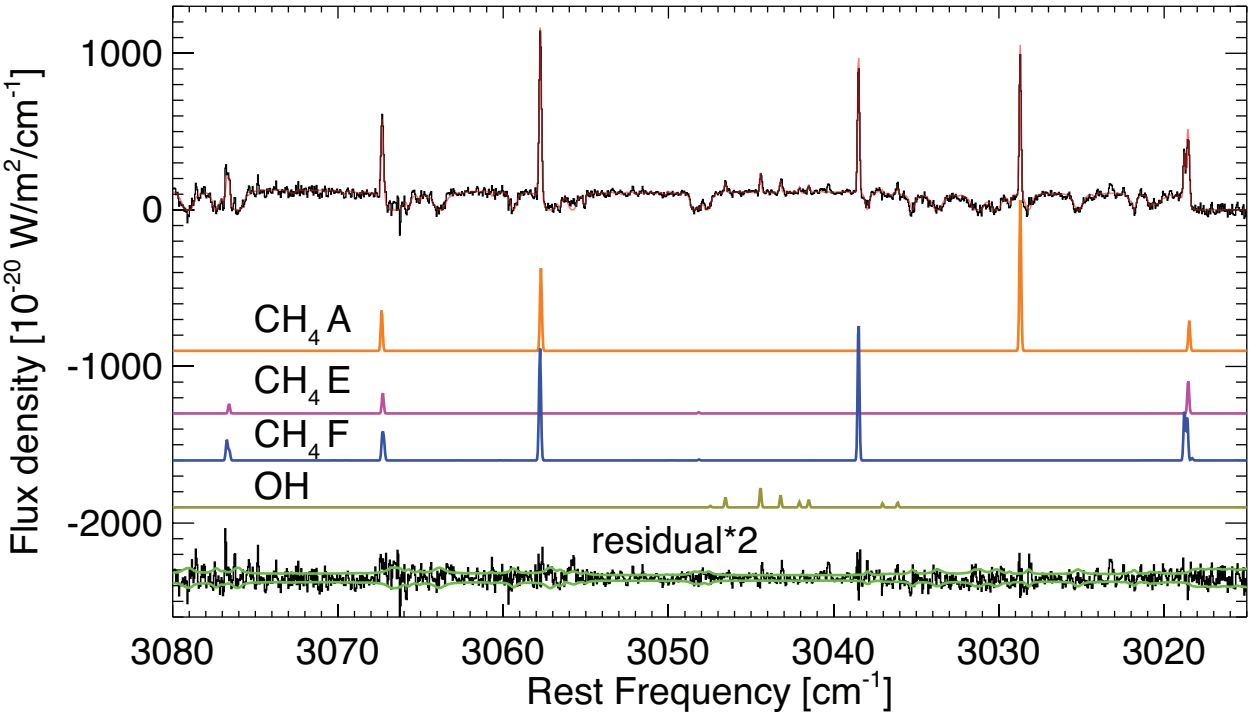

Figure 12: